Catalysis Today 420 (2023) 114140

Contents lists available at ScienceDirect

Catalysis Today

journal homepage: www.elsevier.com/locate/cattod

Perspectives on current and future iridium demand and iridium oxide catalysts for PEM water electrolysis

Mark Clapp [a,*], Christopher M. Zalitis [a,*], Margery Ryan [b]

[a] Johnson Matthey Technology Centre, Blounts Court Rd, Sonning Common, Reading RG4 9NH, UK
[b] Johnson Matthey PGMS, Orchard Road, Royston, Herts SG8 5HE, UK

ARTICLE INFO

Keywords:
Proton exchange membrane water electrolysis
Polymer electrolyte membrane water electrolysis
Iridium
Oxygen evolution reaction
Electrocatalysis
Technoeconomics
Iridium demand
Iridium supply
PEM capacity projection
Critical raw material
Green hydrogen
Electrolytic hydrogen
Clean hydrogen
Iridium recycling
Iridium utilisation
Electrolysis efficiency

ABSTRACT

Proton exchange membrane water electrolysis (PEMWE) is projected to become a key technology to enable the decarbonisation of 'hard to abate' sectors of the economy. However, the technology's reliance on iridium, one of the scarcest elements on Earth, as an oxygen evolution reaction catalyst, has led to uncertainty over whether a large-scale PEMWE industry can be realised. This work investigates the future iridium demand of the global PEMWE sector and examines how different catalyst strategies can improve iridium utilisation in the anode catalyst. Iridium utilisation targets necessary to avoid a situation where the PEMWE sector becomes limited by iridium supply are reviewed. Modelling the iridium demand of the PEMWE sector shows that iridium utilisation needs to improve by an order of magnitude by 2050 to avoid iridium supply limiting the capacity expansion. Furthermore, implementing closed-loop iridium recycling by 2035 would increase the installed capacity in 2050 by ~2.7x compared to a scenario with no iridium recycling. If these two conditions are met, global PEMWE capacity could reach 1.3 TW by 2050 using only 20% of annual global primary iridium supply, which we consider to be realistic given future demand projections. Different types of iridium-based anode catalysts are compared in terms of iridium utilisation using membrane electrode assembly (MEA) testing data from the literature, with the order found to be supported nanoparticles ≈ extended surface structures > mixed oxides > nanoparticles. The need to place greater research focus on catalyst stability and the ability to make homogeneous catalyst layers at low iridium loadings is discussed. As a main result, it is found that a terrawatt-scale PEMWE industry can avoid being constrained by iridium supply if technological development of a similar level to that seen in PEM fuel cells and high iridium recycling rates are realised.

1. Introduction

Hydrogen produced using power from renewable sources, colloquially known as "green hydrogen", is expected to be a key factor in decarbonising the global economy. Green hydrogen can act both as an energy vector, for example as a fuel for heavy-duty vehicles, and as a sustainable chemical feedstock [1]. Proton exchange membrane water electrolysis (PEMWE) is particularly well suited to this task due to its high power density and fast load-following capability, and is expected to make up 40% of the green hydrogen market [2,3]. Several studies, including those by the International Energy Agency (IEA) [4–6], the International Renewable Energy Agency (IRENA) [7], the Hydrogen Council [1] and the German government [2] have projected rapid increases in green hydrogen production *via* water electrolysis in the next few decades, if decarbonisation pledges are to be met. These studies vary in the way they project electrolysis capacity to increase. In this work, the IEA's Announced Pledges Scenario (APS) projection [5] was used as a conservative capacity increase scenario, while the IEA's Net Zero Emissions by 2050 scenario (NZE) [5] and the Hydrogen Council's projections were used as more ambitious options (Fig. 1, with formulae and assumptions in the Supporting Information (SI)). In the IEA APS, which is based on all announced national targets to reduce emissions, PEMWE capacity will need to increase from today's 0.3 GW to ~80 GW by 2030 and ~580 GW by 2050. The IEA NZE requires capacity to grow to ~220 GW by 2030 and ~1130 GW by 2050.

Iridium oxide (IrO_x) is used to catalyse the kinetically unfavourable anodic oxygen evolution half-reaction (OER) during PEMWE, as it provides the best balance of activity and stability under PEMWE conditions [8]. However, iridium supply is constrained and inelastic, as iridium is a minor by-product of mining for other platinum-group metals (PGMs),

* Corresponding authors.
E-mail addresses: mark.clapp@matthey.com (M. Clapp), chris.zalitis@matthey.com (C.M. Zalitis).

https://doi.org/10.1016/j.cattod.2023.114140
Received 5 December 2022; Received in revised form 10 March 2023; Accepted 1 April 2023
Available online 5 April 2023

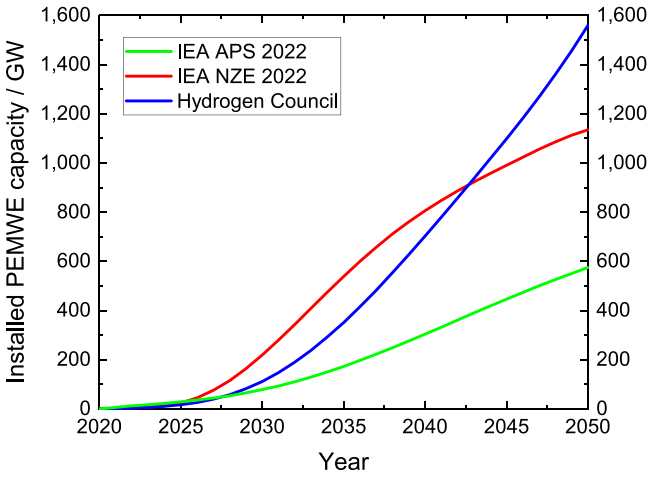

Fig. 1. Projected global PEMWE capacity derived from data from the IEA APS [5] (green line), IEA NZE [5] (red line) and the Hydrogen Council [1] (blue line). For assumptions and details on how the targets were derived, see Section S1 in the SI.

predominantly platinum mining in southern Africa, which is the source of over 90% of primary iridium supplied to the market annually [9]. Indeed, iridium typically accounts for only 2–4% of the overall PGM grade in the ore [9]. In the absence of a significant expansion of platinum mining in this region, mined iridium supply is not expected to increase above the current level of around 7–8 t yr^{-1} [9]. As such, and given competing demands for the metal for spark plugs, ballast water treatment, process catalysts for acetic acid plants, copper foil manufacturing for lithium batteries and making crystals for the electronics industry, iridium supply has the potential to limit the deployment of PEMWE capacity, unless the efficiency of iridium use in the technology is maximised. Although PEMWE also uses platinum as the cathode catalyst, platinum supplies are not expected to limit PEMWE capacity growth, since the global supply of platinum is much larger (~190 t yr^{-1}) and more elastic than for iridium [9]. Furthermore, the thrifting of platinum in the cathode is more advanced than iridium on the anode due to extensive R&D in the hydrogen fuel cell area. Therefore, this work considers only iridium's potential to limit PEMWE expansion.

There are relatively few studies on the feasibility of a large-scale PEMWE industry in terms of iridium demand. A study [10] commissioned by the German Mineral Resources Agency (DERA) examined PEMWE iridium demand based on the Shared Socioeconomic Pathways (SSPs) defined by the Intergovernmental Panel on Climate Change (IPCC) [11]. The study found that by 2040, the global annual iridium demand for PEMWE will reach 10 t yr^{-1} in the SSP2 ('Middle of the Road') and 34 t yr^{-1} in the SSP1 ('Sustainability – Taking the Green Road'). Clearly, demand volumes of these magnitudes would place a severe limitation on the expansion of PEMWE capacity. However, the impact of iridium recycling from end-of-life (EoL) membrane electrode assemblies (MEAs) was not included in the calculations. Furthermore, a fixed value of iridium utilisation (iridium needed per mass of hydrogen produced) was assumed, meaning that the potential for R&D to improve the technology was not taken into account.

A study by the Netherlands Organisation for Applied Scientific Research (TNO) [12,13] identified iridium as the most constrained critical raw material for PEMWE and found that improved iridium utilisation in MEAs could reduce the EU's PEMWE demand in 2050 from 122% of global annual primary supply to only 6%. A recent study on the industrialisation of water electrolysis in Germany (IndWEDe) [2], commissioned by the Federal Ministry for Digital and Transport (BMDV), went into further detail by assuming a continuous improvement in iridium utilisation in their innovative scenario when modelling the iridium demand of the German PEMWE sector. Kiemel *et al.* [3] and Minke *et al.* [14] built on these studies by introducing effective iridium recycling within the German and global PEMWE sectors, respectively. Minke *et al.* concluded that, with effective recycling and a dramatic reduction of iridium loadings on MEAs, a global PEMWE capacity on the order of 100 GW can be reached by 2050 without placing undue pressure on iridium supplies. However, this study assumed a single, stepwise reduction in iridium utilisation from 0.33 mg_{Ir} W^{-1} to 0.05 mg_{Ir} W^{-1} in 2035, which is not realistic.

Developing on these previous studies, in the first half of this paper a detailed model of global future iridium demand for GW- and TW-scale deployment of PEMWE is presented. This study aims to provide the most comprehensive analysis of global PEMWE iridium demand to date by including the effects of improvement in iridium utilisation with time, effective iridium recycling and MEA lifetime extension. The model makes realistic assumptions for other variables based on the literature and includes sensitivity studies. This enables us to project the possible future size of the PEMWE sector and the conditions necessary for it to be realised.

In order to achieve the required improvement in iridium utilisation, advancements in the performance of the PEMWE OER catalysts will be necessary. OER catalysts based on iridium can vary in terms of morphology, crystallinity, surface area, support material and composition. Several studies have reviewed the different types of iridium-based catalysts developed for PEMWE and their ability to improve iridium utilisation [15–23].

The second half of the paper gives an overview of the various technological levers that can be used to improve iridium utilisation, focusing particularly on the OER catalyst. The performances in the real-world application of different catalyst types from the literature are directly compared by normalising some of the resistances expected in a MEA. The advantages and disadvantages of the different catalyst types in improving iridium utilisation are discussed, and the most promising strategies identified.

2. Iridium-specific power density targets

The efficiency of iridium use is improved by obtaining the maximum catalytic activity from each iridium atom in the catalyst, *i.e.* maximising the iridium utilisation.

A useful way of measuring iridium utilisation is iridium-specific power density (Ir-PD), which can be defined as the mass in milligrams of iridium required to draw a Watt of nominal power towards hydrogen production in the MEA cell stack of an electrolyser, in units of mg_{Ir} W^{-1}. The nominal power reported here refers to the MEA cell only and does not include balance of plant inefficiencies, with the conversion from system to cell efficiency shown in Fig. 2b.

In order to estimate the future iridium demand of the PEMWE sector, the improvement in iridium utilisation was first modelled. A global overview of Ir-PD targets defined by governmental and intergovernmental bodies (blue and red symbols) and academia (green crosses) was collated and plotted in Fig. 2a [2,7,24–29].

There is no clear consensus as to what constitutes today's (2020–2022) state-of-the-art (SoA) Ir-PD performance, with figures ranging between 0.34 and 2.0 mg_{Ir} W^{-1}. These SoA figures are given by a recent study on the industrialisation of water electrolysis in Germany (IndWEDe) (0.34 mg_{Ir} W^{-1}) [2], the U.S. Department of Energy Hydrogen Program (DoE) (0.53 mg_{Ir} W^{-1}) [24], IRENA (1.3 mg_{Ir} W^{-1}) [7], the EU's Fuel Cells and Hydrogen 2 Joint Undertaking (FCH2JU) [29] and its successor, the Clean Hydrogen Joint Undertaking (CHJU) [28] (2 mg_{Ir} W^{-1}), the Japanese Ministry of Economy, Trade and Industry (METI) (2 mg_{Ir} W^{-1}) [30] and an academic paper by Babic *et al.* (0.5 mg_{Ir} W^{-1}) [25]. There is also scatter in the projected Ir-PD targets going forwards, as there are several assumptions involved in setting such targets, such as the growth of the PEMWE sector, the portion of global green hydrogen production provided by PEMWE, MEA lifetimes and

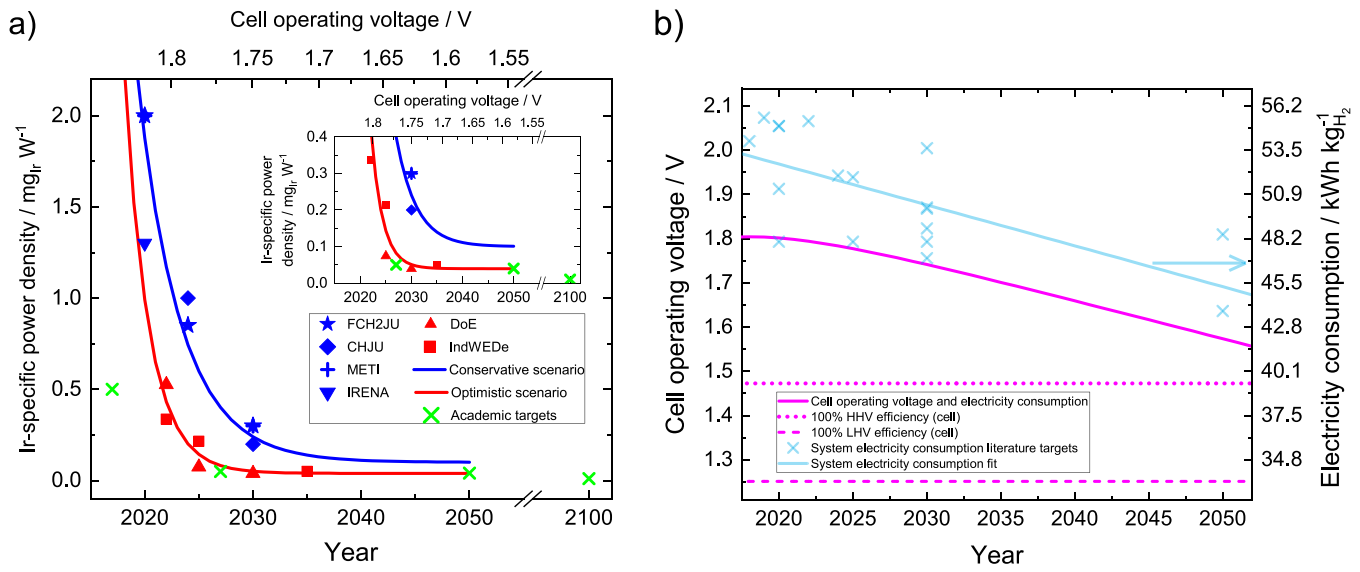

Fig. 2. a) Ir-PD targets collated from governmental/intergovernmental bodies and academia [2,7,24–29], defined at the cell operating voltage at each point in time (top x axis). The blue and red lines show the conservative and optimistic technological development scenarios, respectively. For details of the fitting, see Section S2.4. b) Cell operating voltage and electricity consumption with time (magenta line), which was derived based on literature projections of the electricity consumption of a PEMWE system, shown in light blue (see Section S3.5 for working and Fig. S4 for fitting).

operational loading factors.

Due consideration must be given to MEA lifetime when evaluating performance. While very impressive Ir-PDs can be reached under short-term testing, these power densities may not be sustained over the operational lifetime of a MEA due to catalyst degradation. This could be part of the explanation for the spread in the SoA Ir-PD figures, as the different studies define their SoA performance at different degradation rates, or do not stipulate degradation rates alongside their Ir-PD targets. Ir-PD values with stipulated degradation rates (IndWEDe, DoE, CHJU, FCH2JU, METI) are likely to be more realistic than those that do not consider catalyst degradation explicitly (IRENA, Babic *et al.*). For example, the DoE Ir-PD targets are given alongside a cell degradation rate of 3.2 μV h^{-1} at 2 A cm^{-2} for 2022, which should decrease to 1.6 μV h^{-1} at 3 A cm^{-2} by 2030 [24]. In future, Ir-PD figures should be quoted alongside a MEA degradation rate, to indicate their relevance for commercial PEMWE. A good way of doing this is reporting the increase in cell operating voltage (E_{cell}, V) with time at fixed current density, as done by the DoE. Alternatively, a stability number could be reported, following the work of Geiger *et al.* [31].

Considering the governmental/intergovernmental targets, the IndWEDe and DoE figures (red symbols) are significantly more ambitious than the CHJU, FCH2JU, METI and IRENA figures (blue symbols). To simplify the picture, the IndWEDe and DoE targets were used to model an optimistic technological development scenario, and the CHJU, FCH2JU, METI and IRENA to model a conservative scenario, by fitting exponential decay functions to the targets. Each Ir-PD value along the optimistic and conservative scenario curves is defined at a corresponding cell operating voltage, which decreases with time as shown in Fig. 2b. Fig. 2b was obtained by fitting a line of best fit to system electricity consumption targets from governmental/intergovernmental organisations (see Section S3.5 and Fig. S4 in the SI).

Improving Ir-PD will necessitate decreasing the iridium loadings of MEAs. It has been shown that MEAs with lower loadings can degrade faster and have shorter lifespans due to dissolution of iridium [32] (although MEA lifespan is not solely determined by iridium dissolution). Therefore, for MEAs with lower loadings to have equivalent lifespans, the stability of the catalyst will need to improve. The degree of this improvement will affect what Ir-PD values can be reached and, therefore, what technological development scenario it will follow. In the conservative scenario it was assumed that dissolution would be the limiting factor in Ir-PD reduction. From the work of Yu *et al.* [33] it is possible to estimate that over a 10-year lifespan at a load factor of 0.6 (see Section 3 & 4 for justification), an iridium loading of 0.65 mg$_{Ir}$ cm^{-2} would undergo complete dissolution for their particular catalyst, *i.e.* a minimum loading of 0.65 mg$_{Ir}$ cm^{-2} is currently necessary for a 10-year lifetime (calculation in Section S2.5). Assuming that the stability of the IrO_x catalyst never improves much beyond this, while also accounting for the fact that E_{cell} is projected to decrease in the future (Fig. 2b), leading to less voltage-dependent iridium dissolution, the conservative scenario Ir-PD reduction fitting was constrained to 0.10 mg$_{Ir}$ W^{-1} at 1.58 V (2050 E_{cell}), which corresponds to a loading of 0.23 mg$_{Ir}$ cm^{-2} (see Section S5.1). The optimistic scenario reaches 0.04 mg$_{Ir}$ W^{-1} at 1.58 V using an unconstrained fit, which corresponds to a lower loading limit of 0.10 mg$_{Ir}$ cm^{-2} (see Pathway 4 in Section 6), implying at least a two-fold increase in catalyst stability. It is worth noting that, although these Ir-PD targets may seem very ambitious compared to the current SoA, Ohno *et al.* [34] and Rozain *et al.* [35] have already demonstrated MEA testing results that get very close to these targets, 0.05 mg$_{Ir}$ W^{-1} and 0.09 mg$_{Ir}$ W^{-1} at 1.58 V and 80 °C (values adjusted to 50 μm thick Nafion® 212), respectively (see Fig. 8a). For further details of the fitting, see the SI.

The assumptions employed to derive the academic Ir-PD targets were different to those used by the governmental and intergovernmental organisations. Bernt *et al.* [27] considered the Ir-PD required if green hydrogen were to replace all fossil fuels in the mobility sector, Babic *et al.* [25] assumed a scenario where green hydrogen would act as the major storage vector for all primary energy and Taie *et al.* [26] assumed that green hydrogen would replace the natural gas sector. While these figures provide a useful guide for the necessary technological improvement, these studies assume that 100% of green hydrogen will be produced *via* PEMWE, instead of the 40% figure projected by IndWEDe [2]. Furthermore, they do not explicitly take into account iridium recycling, which can be expected to significantly mitigate the iridium demand of the PEMWE sector [14]. Therefore, these figures were considered to be more speculative than those put forward by governmental/intergovernmental bodies and are hereafter omitted from the modelling.

In the first half of this paper, these two clear Ir-PD technology

development scenarios are used to model the relationship between PEMWE capacity growth and iridium demand, incorporating the effect of recycling. The second half of the paper examines the likelihood of hitting these Ir-PD scenarios, along with strategies for doing so.

3. Modelling PEMWE iridium demand

In this section a model for the future iridium demand of the PEMWE sector is presented and used to calculate the amount of iridium needed to achieve the IEA APS and NZE capacity targets (Fig. 1) for the two technological development scenarios defined in Fig. 2. The assumptions made in the model are shown in Table 1, while the justifications and sensitivity studies for the values assumed can be found in Section S3.

The overall global recycling rate of iridium (*i.e.* the percentage of iridium in EoL components that is recovered for reuse) from industrial processes was estimated in 2011 at 40–50% [36]. Unlike for some industrial uses of iridium (such as spark plugs and ballast water treatment), in PEMWE the iridium is not used up or lost irretrievably. Therefore, the recycling rate from EoL PEMWE MEAs can be expected to be significantly higher than the current average for industrial processes. A useful comparison can be made with PGM recovery rates in autocatalysts, an established recycling route, which stand at around 50–70% today [37,38]. Autocatalysts are recycled in an open-loop system, where ownership of the PGM is not retained by the vehicle manufacturer, resulting in significant losses in collecting EoL autocatalysts, because collection relies on the vehicle owner and scrap recovery network (and recovered metal is sold on the open market). Closed-loop recycling, where ownership of the PGM is retained by either the equipment manufacturer or equipment owner, resulting in them having a strong interest in recovering the PGM, is known to lead to much higher overall recovery rates, all else being equal.

Given that there is insufficient data currently available on iridium recycling rates from EoL PEMWE MEAs, the 2020 overall recycling rate was assumed to be 70%, *i.e.* the upper limit of the autocatalyst recycling range. From there, recycling rates were assumed to increase linearly to maximum rates in 2035, dependent on the nature of the collection approach (open or closed-loop), legislation on product stewardship and varying technical success in flowsheet losses. The base case was assumed to be a scenario where closed-loop recycling is implemented with strict legislation and high technical recycling rates are reached, such as the 97% recovery demonstrated by Carmo et al. [39], increasing the overall recycling rate to the theoretical upper limit of 100% by 2035 for simplicity. Sensitivity studies of the impact of different overall iridium recycling rates are presented in the SI and Section 4. It should be emphasised, however, that these scenarios are not predictions of future recovery rates.

The total iridium demand of the PEMWE sector in year *i* ($\dot{I}r_i^{\text{total demand}}$, t yr^{-1}) necessary to satisfy both the annual rate of new capacity addition in each capacity projection ($\dot{C}_i^{\text{new}}$, GW yr^{-1}) and the replacement of capacity corresponding EoL MEAs ($\dot{C}_i^{\text{replacement}}$) was calculated according to Eq. (1), using the conservative and optimistic Ir-PD functions from Fig. 2. Replacement of capacity that is at EoL is necessary to maintain the same baseline capacity.

$$\dot{I}r_i^{\text{total demand}} = \dot{I}r_i^{\text{new capacity}} + \dot{I}r_i^{\text{replacement}} \tag{1.1}$$

$$\dot{I}r_i^{\text{total demand}} = (\dot{C}_i^{\text{new}} + \dot{C}_i^{\text{replacement}}) \cdot IrPD_i \tag{1.2}$$

where $IrPD_i$ is the Ir-PD in year *i*.

The capacity that needs to be replaced each year was calculated by assuming a normal distribution with a mean of 10 years for the lifetime of MEAs (see the SI for details and a sensitivity study of MEA lifetime). A normal distribution was assumed as it is more realistic than a fixed 10-year lifecycle.

This total iridium demand needs to be satisfied by a combination of recycled and primary (*i.e.* newly-mined iridium, from global annual supply) iridium. The amount of recycled iridium available each year ($\dot{I}r_i^{\text{recycled}}$) was calculated using the normal distribution of MEA lifetimes described above.

$$\dot{I}r_i^{\text{recycled}} = \dot{I}r_{i-\tau}^{\text{total demand}} \cdot \gamma^{\text{recycling}} \tag{2}$$

where $\dot{I}r_{i-\tau}^{\text{total demand}}$ is the total iridium demand of the PEMWE sector in year *i*-τ, with τ varying according to the normal distribution of lifetime, and $\gamma^{\text{recycling}}$ is the overall recycling efficiency.

The annual amount of primary iridium needed ($\dot{I}r_i^{\text{primary}}$) was then calculated according to Eq. (3):

$$\dot{I}r_i^{\text{primary}} = \dot{I}r_i^{\text{total demand}} - \dot{I}r_i^{\text{recycled}} \tag{3}$$

Finally, the cumulative mass of iridium accumulating in the PEMWE sector (Ir_i^{cum}, t) was calculated using Eq. (4):

$$Ir_i^{\text{cum}} = Ir_{i-1}^{\text{cum}} + \dot{I}r_i^{\text{primary}} \tag{4}$$

This model was used to project the evolution of PEMWE iridium demand up to 2050 for the IEA APS and NZE capacity growth projections using the conservative and optimistic technological development scenarios, as shown in Figs. 3 and 4. The equivalent analysis of the Hydrogen Council capacity growth can be found in Section S4, along with sensitivity studies for MEA lifetime, PEMWE market share, load factor and iridium recycling rate.

The iridium demand projections were compared to an iridium availability value of 20% (1.5 t yr^{-1}) of global primary supply (dashed red lines). Although currently all iridium mined annually is already accounted for by other sectors [9], there is considerable potential for demand reduction in uses such as spark plugs for internal combustion engines, where replacement with platinum is a possibility. Therefore, we consider 20% of annual primary supply being available for PEMWE without placing unsustainable pressure on iridium supplies to be a

Table 1
Assumptions used for modelling PEMWE iridium demand and capacity growth. For the literature background that these values are based on, see the SI.

Annual global primary iridium supply[a] [9]	7.5 t yr^{-1}
Iridium recycling rate from EoL MEAs	linear rise: 70% in 2020 to 100% in 2035
MEA lifetime (τ) [7,28]	10 years (normal distribution, see SI)
Load factor [40]	0.6
PEMWE green hydrogen market share [2,3]	40%
System electricity consumption (see Fig. 2a)	2022: 52.2 kWh $kg_{H_2}^{-1}$ to 2050: 45.3 kWh $kg_{H_2}^{-1}$

[a] Note that, besides mining and recycling, iridium could also be sourced from stocks (if any) and other sources of 'above-ground' metal, potentially including from current applications. However, for the purposes of this work, the only sources considered are mining (primary source) and recycling of iridium from EoL electrolysers.

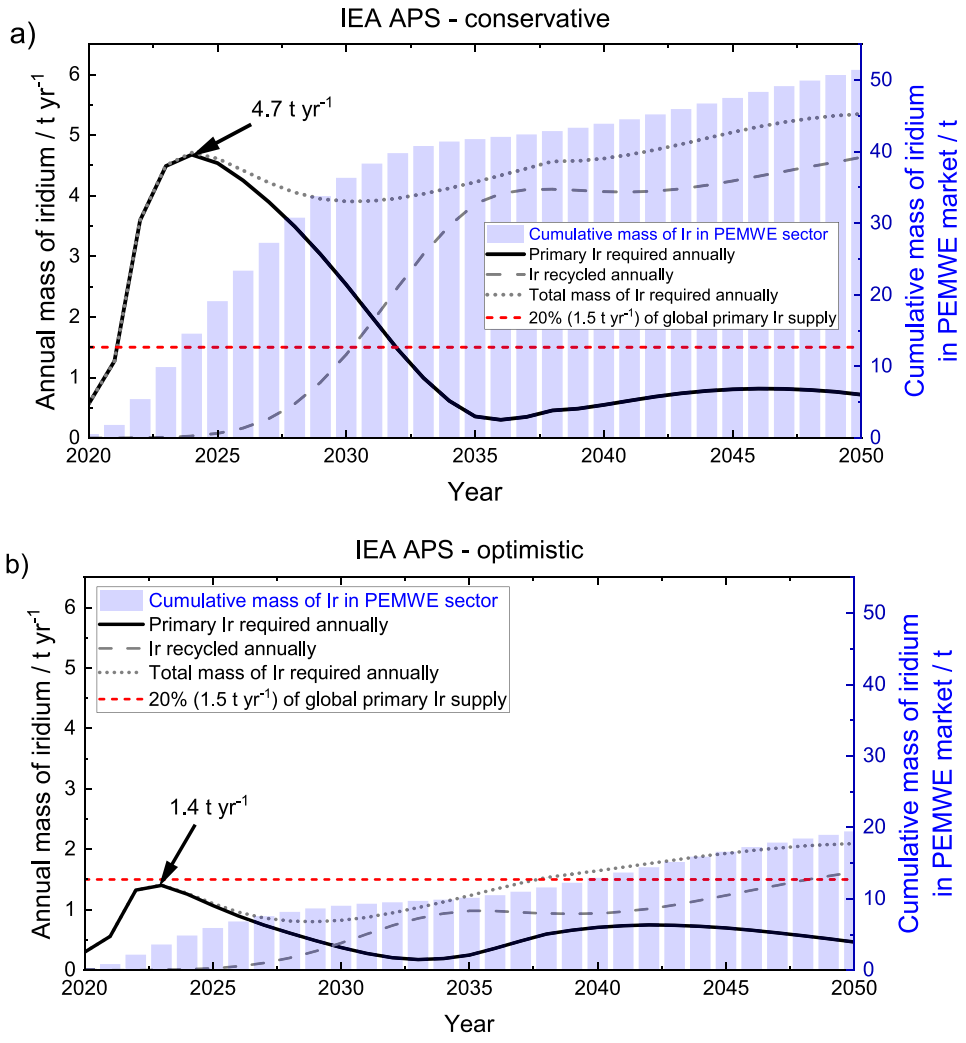

Fig. 3. Annual iridium demand, amount of recycled iridium and cumulative build-up of iridium over time in the PEMWE market in the IEA APS, considering the a) conservative and b) optimistic scenario of Ir-PD improvement (Fig. 2). Assumptions shown in Table 1.

realistic value based on internal modelling [38].

The iridium demand functions shown in Figs. 3 and 4 are convolutions of the PEMWE capacity growth and the Ir-PD functions. The evolution of the primary iridium demand (solid black lines) is similar for both the APS and NZE in their respective conservative and optimistic technological development scenarios, as primary demand peaks pre-2030, before decreasing significantly up to 2050. The peaks are caused by the rapid ramps in capacity while Ir-PD is still relatively high and the fact that a lack of EoL MEAs means recycling has not yet taken effect. The dramatic primary demand reductions after the peaks are due to rapid improvement in Ir-PD and significant amounts of recycled iridium (dashed black lines) starting to circulate in the sector, easing the pressure on primary iridium supplies.

Fig. 3a shows that in order to meet the IEA APS forecast in the conservative scenario and with the stated assumptions, demand for primary iridium would peak at 4.7 t $year^{-1}$ in 2024 (~62% of global annual supply), before decreasing rapidly up to the mid-2030s. Given current iridium demand in other sectors [9], a 62% share for PEMWE in 2024 is unrealistic. On the other hand, primary demand dips below the 20% threshold by 2032, and remains comfortably below it through to 2050. Indeed, the cumulative primary iridium demand up to 2050 would be only 23% of the cumulative global supply over the same time period (Table 2). Therefore, while in the conservative scenario the APS would be limited by iridium supply in the near-term, more gradual capacity growth with a comparable final magnitude in 2050 would likely be possible.

In the APS's optimistic scenario (Fig. 3b), primary iridium demand follows a similar pattern to the demand in the conservative scenario, but with demand never rising above the 20% threshold through to 2050. The cumulative primary demand up to 2050 would only be 9% of cumulative supply. This is a significant finding, suggesting that if the optimistic scenario of technological development were realised, the IEA APS capacity projection would not be limited by global iridium supply.

Fig. 4a shows that, if the conservative technological development scenario is assumed, the NZE's primary iridium demand would peak at 13 t yr^{-1} in 2028. This is unrealistically high, meaning that the NZE capacity projection would be limited by iridium supply. It should be noted that although the PEMWE sector would be self-sufficient after 2038 due to the aggressive nature of the initial capacity increase leading to very large quantities of iridium re-circulating through recycling, primary iridium demand would once again materialise at some point after 2050 if the total capacity continued to grow and technological progress plateaued.

On the other hand, if the optimistic scenario is assumed, the NZE projection would be significantly more attainable (Fig. 4b). Although primary demand would be above the 20% threshold between 2025 and 2035, it would peak at only 2.5 t yr^{-1}, or 34% of supply, and may be at a level that can be absorbed for a period of 10 years. After 2035, primary

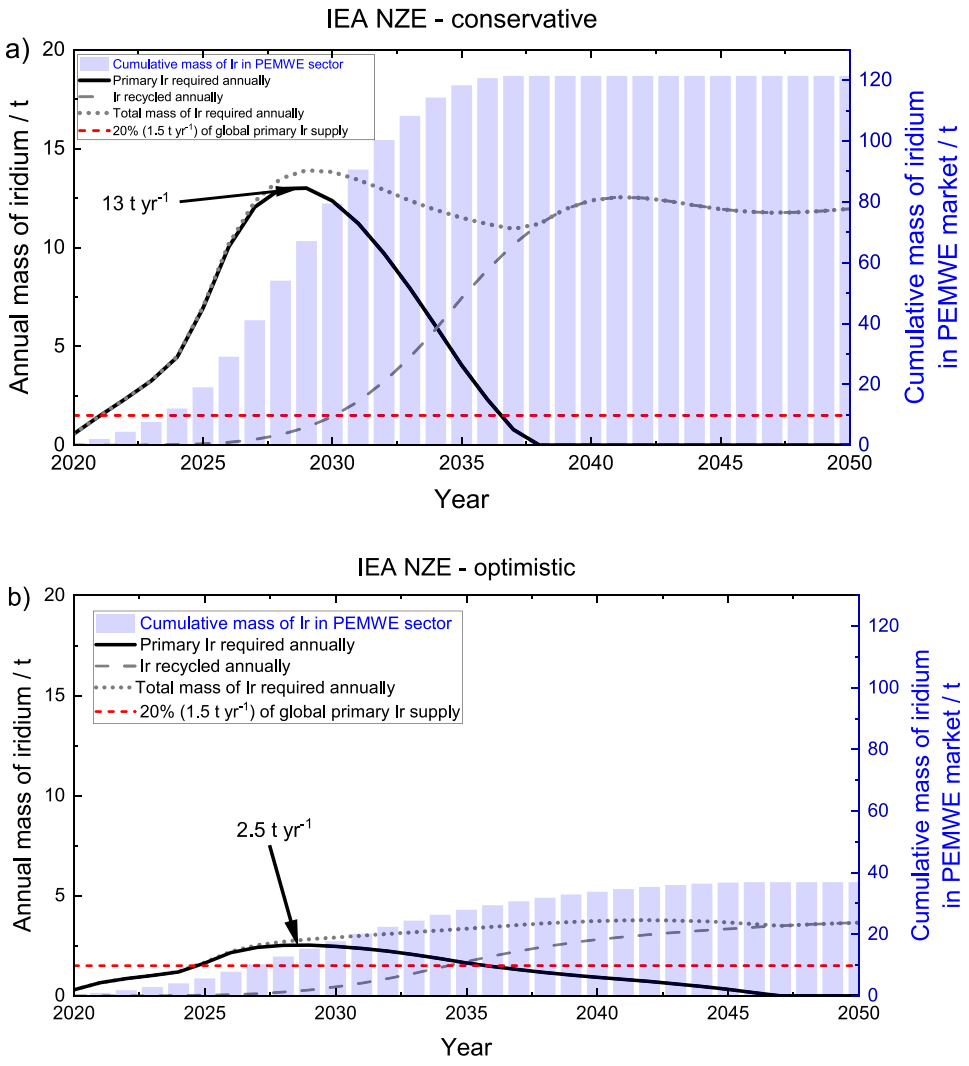

Fig. 4. Annual iridium demand, amount of recycled iridium and cumulative build-up of iridium over time in the PEMWE market in the IEA NZE, considering the a) conservative and b) optimistic scenario of Ir-PD improvement (Fig. 2). Assumptions shown in Table 1.

Table 2
Key results for IEA APS and NZE iridium demand (Figs. 3 and 4).

	IEA APS PEMWE capacity target		IEA NZE PEMWE capacity target	
	Conservative	Optimistic	Conservative	Optimistic
Peak in primary iridium demand / t yr^{-1}	4.7	1.4	13	2.5
% of cumulative primary iridium supply required by PEMWE sector up to 2050	23	9	54	16

demand would remain below the 20% threshold through to 2050, gradually decreasing to zero as the PEMWE sector becomes self-sufficient in terms of iridium thanks to effective recycling of the iridium involved in the initial capacity growth. Indeed, the cumulative primary demand up to 2050 is only 16% of cumulative global supply (Table 2), meaning that if the initial surge in demand can be absorbed by the market, the NZE capacity projection in the optimistic scenario could be realised in the long term without placing undue pressure on iridium supply.

The pre-2030 peak in iridium demand is present in all the permutations considered in Figs. 3 and 4. This implies that an expansion in PEMWE capacity that is more gradual up to 2030, but accelerates rapidly once iridium has accumulated in the sector, would represent a growth trajectory that would place less pressure on primary iridium supply, while still reaching a high capacity by 2050. This is illustrated by the comparison between the Hydrogen Council and IEA NZE targets in Fig. 1, where the Hydrogen Council's capacity projection grows at a slower rate up to 2036, but significantly faster after that. Distributing the capacity growth in this way allows, in the optimistic scenario, for the Hydrogen Council's projection to have a similar level of attainability in terms of iridium demand as the NZE (see Fig. S11 in the SI), despite reaching a 2050 total capacity that is 38% higher.

It should be noted that using MEAs with shorter lifetimes could also help reduce the width of the pre-2030 peak and increase early-stage capacity growth, as the iridium locked up in MEAs would cycle through the recycling system earlier and would therefore be available for incorporation into new MEAs earlier. As the reincorporation of iridium is using the newer Ir-PD, it not only covers the capacity it is replacing but can be used for additional capacity. This is shown in the sensitivity studies in Fig. S7 and S8.

The PEMWE green hydrogen market share and the load factor affect the magnitude of the PEMWE capacity projections, with their iridium demand changing accordingly in the sensitivity studies shown in Figs. S5 and S6.

4. Modelling PEMWE capacity growth

In this section, the potential capacity growth assuming a constrained primary iridium supply into the PEMWE sector was modelled. The model from Section 3 was used, but with the inverse equations, *i.e.* calculating the capacity addition possible from a given iridium supply, which are given briefly here. The assumptions are given in Table 1.

First, the new capacity addition in year i ($\dot{C}_i^{primary}$) enabled by a given amount of primary iridium ($\dot{Ir}_i^{primary}$) was calculated:

$$\dot{C}_i^{primary} = \frac{\dot{Ir}_i^{primary}}{IrPD_i} \tag{5}$$

Then, capacity that could be added using recycled iridium was calculated according to Eq. (6):

$$\dot{C}_i^{recycled} = \frac{\dot{Ir}_{i-\tau}^{total\ demand} \cdot \gamma^{recycling}}{IrPD_i} \tag{6}$$

Eq. (6) highlights how the capacity added τ years previously can be replaced with less iridium than was necessary at installation due to the improvement in Ir-PD with time (see Fig. 2).

The new capacity added in each year was then obtained by subtracting the capacity that must be replaced:

$$\dot{C}_i^{new} = \dot{C}_i^{primary} + \dot{C}_i^{recycled} - \dot{C}_i^{replacement} \tag{7}$$

where $\dot{C}_i^{replacement}$ was again calculated using the normal distribution for MEA lifetimes.

The total capacity can then simply be calculated according to Eq. (8):

$$C_i^{total} = C_{i-1}^{total} + \dot{C}_i^{new} \tag{8}$$

Sensitivity studies for MEA lifetime, PEMWE market share, load factor and iridium recycling rate can be found in this section and the SI.

Fig. 5 shows the capacity increase made possible by given fractions of global annual primary iridium supply being available for the PEMWE sector, for both the conservative and optimistic technological development scenarios, again assuming that the recycling efficiency of iridium from EoL MEAs rises from 70% in 2020 to 100% in 2035.

Fig. 5a shows that, in the conservative scenario, a realistic 20% share of the primary iridium supply would enable 466 GW of PEMWE capacity to be installed by 2050 (orange line). This is close to the 577 GW targeted by the IEA APS; indeed, it would be possible to match the 2050 APS capacity target if ~25% of primary iridium (1.8 t yr^{-1}) were used for PEMWE each year. Although this is slightly above the 20% threshold discussed in the previous section, nonetheless it is still a relatively realistic level of demand.

Fig. 5b shows that, in the optimistic scenario, the 20% primary supply share would allow 1.3 TW of installed capacity by 2050 (orange line). This is a significant finding, as it means that if optimistic technological advancement and recycling efficiency rising from 70% in 2020 to 100% in 2035 onwards is assumed, the PEMWE capacity would surpass the IEA NZE capacity target from 2045 onwards using only 20% of global supply. From 2032 onwards, the less ambitious IEA APS would be achieved using < 10% of global primary iridium supplies annually. This underlines the importance of improving the Ir-PD of PEMWEs through research and development.

Fig. 6 shows a sensitivity study of the recycling efficiency of iridium from EoL MEAs, with the primary iridium input constrained at 20% of global supply. Recycling has a significant impact on PEMWE capacity growth. If no recycling is taken into account, global capacity would reach 173 and 505 GW by 2050 in the conservative and optimistic scenarios, respectively. If recycling rates were to stay at today's assumed rate of 70% (*i.e.* open-loop with no further development in recycling), global capacity would increase to 348 and 985 GW by 2050. If recycling rates develop further in the future from today's 70% to 100% (closed-loop) by 2035, global capacity would further increase to 466 GW and 1.3 TW. Compared to a future pathway with no recycling, this is a 2.7x and 2.6x increase in capacity by 2050 for the conservative and optimistic technological development scenarios, respectively (Table 3). This shows the importance of improving the technical processes for recycling iridium and the vital role that policy and legislation that encourages closed-loop recycling will play in the growth of PEMWE capacity. If the theoretical upper limit of 100% is not reached by 2035, a maximum recycling rate of 80% and 90% would still result in the optimistic scenario 2050 capacity increasing 2.2x and 2.4x, respectively, compared to the case with no recycling.

It is also noted that in the optimistic scenario, the 2050 IEA APS target (577 GW) is almost achieved with no recycling taken into account (505 GW) (red and solid black lines in Fig. 6b), using only 20% of global

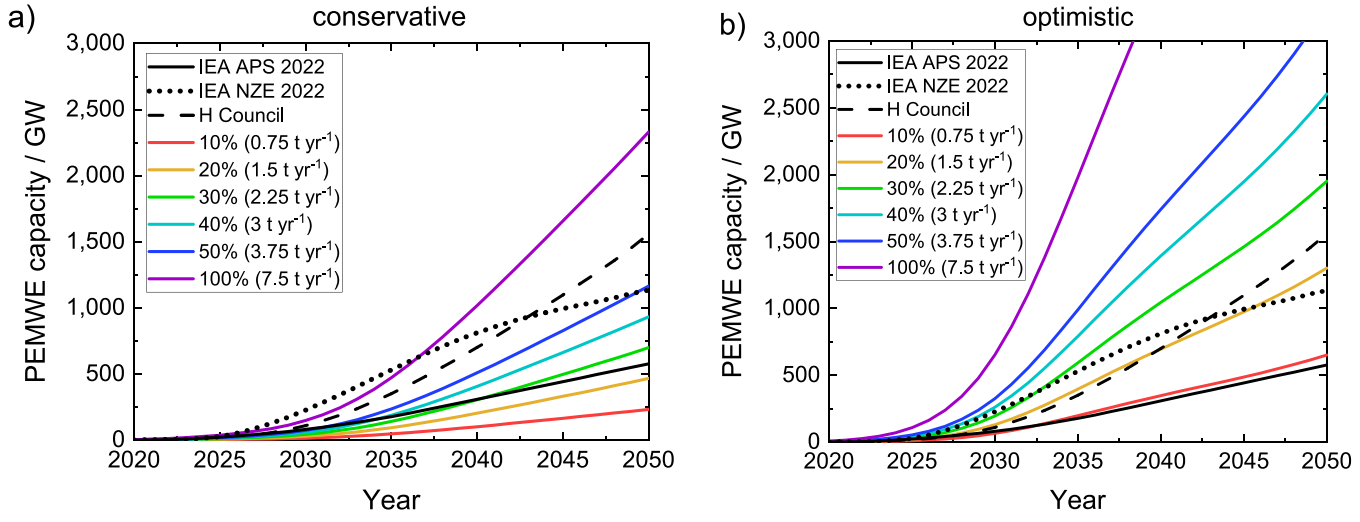

Fig. 5. Global PEMWE capacity increase if the mass of primary iridium available to the PEMWE sector annually is constrained at various values, considering the a) conservative and b) optimistic scenario of Ir-PD improvement (Fig. 2). The IEA APS, IEA NZE and Hydrogen Council projected capacities are included for comparison. Assumptions shown in Table 1. Versions of the graphs with insets showing the capacity growth between 2020 and 2035 are in the SI, Fig. S10.

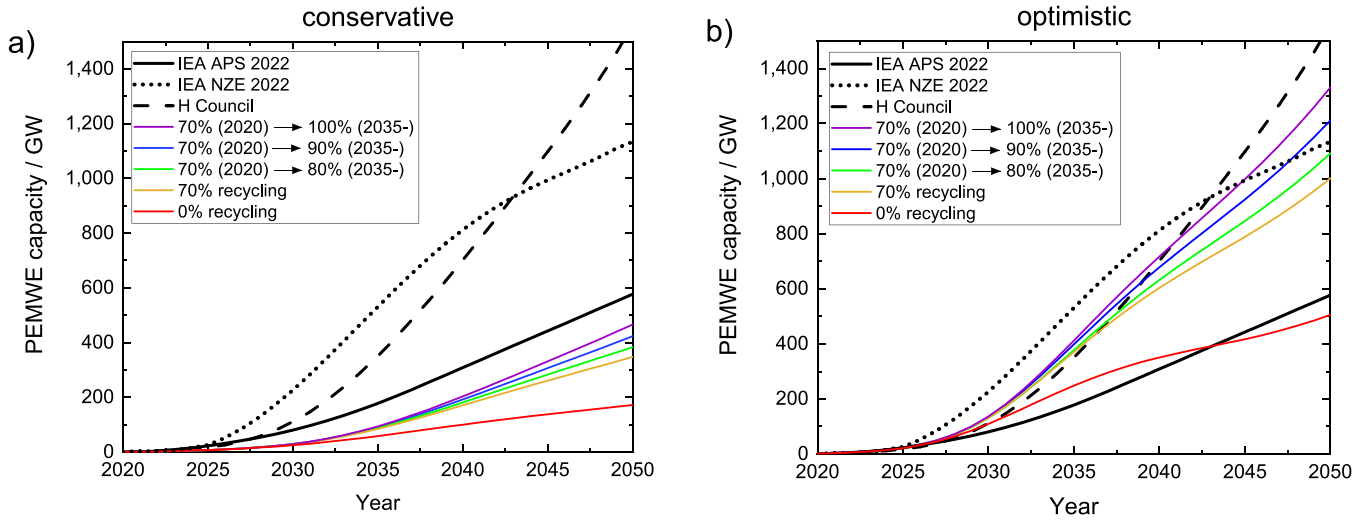

Fig. 6. Sensitivity study of the effect of iridium recycling rates from EoL MEAs on global PEMWE capacity increase considering a a) conservative and an b) optimistic scenario of Ir-PD improvement (Fig. 2). The mass of primary iridium available to the PEMWE sector annually is constrained at a fixed value of 20% of annual global primary supply (1.5 t yr^{-1}). The IEA APS, IEA NZE and Hydrogen Council projected capacities are included for comparison. Assumptions shown in Table 1.

Table 3
Key results for PEMWE capacity with a constrained primary iridium input (Figs. 5 and 6).

	2050 PEMWE capacity (20% iridium supply, recycling: 70% in 2020 →100% in 2035)	2050 capacity increase for recycling 70% in 2020→100% in 2035 compared to no recycling
Conservative scenario	466 GW	2.7x
Optimistic scenario	1302 GW	2.6x

iridium supply. This is significant as it shows that, although recycling would enable a much larger PEMWE industry, the future development of a large PEMWE industry is not predicated on iridium recycling, assuming that the optimistic reduction in Ir-PD can be met.

The analysis presented in this section has shown that as long as sufficient improvements in Ir-PD and high iridium recycling rates (>90%) are achieved, a global PEMWE capacity of well over 1 TW can be achieved by 2050 without being limited by iridium supply.

5. Technological levers to reduce iridium-specific power density

Based on Fig. 2, reductions in Ir-PD by at least a factor of 10 will be necessary to enable the rapid expansion of PEMWE without being limited by primary iridium supply, for both the conservative and optimistic scenario. The second half of this paper examines the technological levers that can be used to achieve these reductions in Ir-PD at the MEA level. MEA includes any configuration of the electrodes used in water electrolysis encompassing structures such as catalyst coated membranes (CCMs) and catalyst coated substrates (CCSs). In general, when Ir-PD targets and associated MEA performances are discussed, they are defined at the operational cell voltage values (E_{cell}, see Fig. 2b) corresponding to their associated timepoint in the future. However, this makes comparison of future performances to each other and to literature testing difficult, because E_{cell}, the driving force of the reaction, is not constant. Therefore, to aid comparison, in the rest of the paper Ir-PD values and MEA performance metrics, such as resistive losses and current densities, are sometimes defined at a common E_{cell} of 1.79 V (= 70% lower heating value (LHV) efficiency), which is used by other relevant publications as a reference voltage [27,41–43]. The normalisation is discussed in Section S6 and the reference voltage is made clear in each instance.

The Ir-PD of a PEMWE can be calculated using Eq. (9), where the right-hand side of the equation shows that Ir-PD can be lowered by increasing the iridium mass-specific current (j_{mass}, Amg_{Ir}^{-1}) while keeping the cell voltage (E_{cell}, V) fixed:

$$\text{Ir} - \text{PD} = \frac{1}{j_{mass} \cdot E_{cell}} \tag{9}$$

where

$$j_{mass} = \frac{j_{geo}}{L_{Ir}} \tag{10}$$

and j_{geo}: geometric current density (A cm^{-2}), L_{Ir}: iridium loading of the MEA (mg_{Ir} cm^{-2}).

E_{cell} can be split into individual contributions as shown in Eq. (11):

$$E_{cell} = E_{eq}^{OER} + \eta_{kin}^{OER} + j_{geo} \cdot (R_{kin}^{HER} + R_{memb} + R_{el} + R_{an} + R_{cath} + R_{mt}) \tag{11}$$

where E_{eq}^{OER}: equilibrium potential for the OER (anodic half reaction), η_{kin}^{OER}: OER kinetic overpotential, R_{kin}^{HER}: resistance associated with the hydrogen evolution reaction (HER, cathodic half reaction) kinetic overpotential (Ω cm^2), R_{memb}: PEM resistance, R_{el}: electronic resistance due to the bipolar plate, porous transport layer (PTL) *etc.*, R_{an} and R_{cath}: resistance due to the anode and cathode catalyst layers (CLs), respectively, and R_{mt}: mass transport resistance.

In simplifying E_{cell} to Eq. (11), η_{kin}^{HER} was linearised. This is reasonable as several studies have shown that the HER is extremely facile on Pt/C and, therefore, the reaction is likely to be very close to the equilibrium potential even at current densities as high as 3 A cm^{-2} (η_{kin}^{HER} = 7 mV in Fig. 7). This means that the current density can be expressed as a linear function of η_{kin}^{HER} [44–46], such that η_{kin}^{HER} can be represented as the Ohmic resistive term $j_{geo} \cdot R_{kin}^{HER}$.

All the Ohmic resistances in Eq. (11) can then be represented as a single resistance (R_{cell}), allowing it to be re-written as:

$$E_{cell} = E_{eq}^{OER} + \eta_{kin}^{OER} + j_{geo} \cdot R_{cell} \tag{12}$$

where $\eta_{kin}^{OER} + j_{geo} \cdot R_{cell}$ is the total overpotential applied.

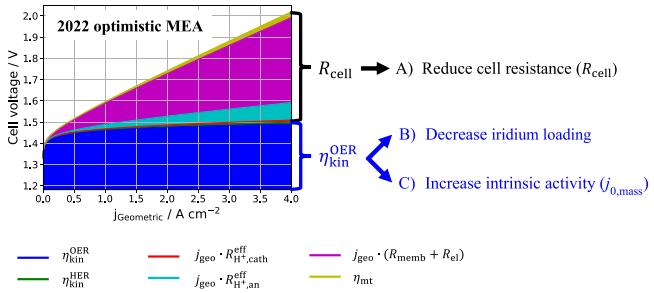

Fig. 7. Deconvoluted overpotentials for a current SoA MEA, see Tables 4 and 6 for assumptions and parameters. The technological levers for reducing Ir-PD are also shown.

j_{geo} for a PEMWE MEA can be modelled based on the anodic Butler-Volmer equation:

$$j_{geo} = j_{0,geo} \cdot \exp\left(\frac{\alpha_{OER} z F}{RT} \cdot \eta_{kin}^{OER}\right) \quad (13)$$

where j_{geo}: geometric exchange current density, α_{OER}: anodic charge transfer coefficient, z: number of electrons involved in reaction, F: Faraday constant (C mol^{-1}), R: universal gas constant (J K^{-1} mol^{-1}), T: temperature (K).

Finally, the mass-specific polarisation curve for a PEMWE MEA can be modelled by rearranging Eq. 12 for η_{kin}^{OER} and substituting into the mass-specific analogue of Eq. (13):

$$j_{mass} = j_{0,mass} \cdot \exp\left(\frac{\alpha_{OER} z F}{RT} \cdot \eta_{kin}^{OER}\right) \quad (14)$$

$$j_{mass} = j_{0,mass} \cdot \exp\left(\frac{\alpha_{OER} z F}{RT} \cdot \left(E_{cell} - E_{eq}^{OER} - j_{geo} \cdot R_{cell}\right)\right) \quad (15)$$

Based on Eq. (15), at a given E_{cell}, j_{mass} can be increased (and Ir-PD reduced) using the following technological levers:

A) Reducing R_{cell} at fixed loading and $j_{0,mass}$, which effectively increases the η_{kin}^{OER} by reducing $j_{geo} \cdot R_{cel}$, *i.e.* more of the total overpotential is applied directly to the catalyst (higher η_{kin}^{OER}), resulting in a higher j_{mass};
B) Reducing loading at fixed $j_{0,mass}$ and R_{cell}, which again effectively increases the η_{kin}^{OER} applied to the catalyst;
C) Increasing $j_{0,mass}$ at fixed loading and R_{cell}, *i.e.* improving the intrinsic activity of the catalyst.

The various overpotentials in Eq. (11) can be deconvoluted using values from Bernt and Gasteiger [47] to examine levers A, B and C for reducing Ir-PD. The deconvoluted overpotentials for a representative current SoA electrolyser were plotted in Fig. 7 using literature values for the activity and resistance descriptors, which are shown in Tables 4 and 6. R_{an} and R_{cath} were considered as protonic resistances only ($R_{H^+,an}^{eff}$ and $R_{H^+,cath}^{eff}$), as at the relevant ionomer loadings protonic resistance dominates the electronic resistance [48]. The Tafel slope ($\frac{RT}{\alpha_{OER} zF}$) was assumed to be constant, *i.e.* the same OER mechanism was assumed for all iridium-based catalysts (Table 4). For more details on the deconvolution, see Section S5.

Table 4
Parameters used in the MEA model. The PEM conductivity may change significantly in the future if alternative technologies such as hydrocarbon membranes are developed.

Parameter	Value
Tafel slope (IrO_x value at 80 °C corresponding to [47,49])	45 mV dec^{-1}
Operating temperature (T)	80 °C
Operating pressure	Atmospheric, balanced
OER equilibrium potential (E_{eq}^{OER})	1.18 V
PEM conductivity (Nafion®) [47]	142 mS cm^{-1}
A) R_{cell}, which is dominated by R_{memb}	See Table 6 and S14
B) MEA iridium loading (L_{Ir})	See Table 6
C) Intrinsic catalyst activity ($j_{0,mass}$)	See Table 6

The largest contribution by far to the total overpotential at 2 A cm^{-2} is due to the OER kinetic overpotential (η_{kin}^{OER}, dark blue wedge in Fig. 7), which contributes ~54% of the total for current SoA MEAs at 1.79 V. Clearly, the anodic IrO_x catalyst is critical for reducing Ir-PD using levers B and C. A secondary effect of decreasing the iridium loading (lever B) is that a thinner CL may lead to a lower $R_{H^+,an}^{eff}$ (teal wedge in Fig. 7), which at ~7% is the third largest contributor to the total overpotential at 2 A cm^{-2}. The catalyst strategies that can use levers B and C to reduce Ir-PD are the focus of Sections 6-8.

The second largest overpotential is due to membrane resistance ($j_{geo} \cdot R_{memb}$, purple wedge in Fig. 7), which contributes ~30% of the overpotential at 1.79 V for current SoA MEAs. Reducing the thickness or increasing the conductivity of the PEM lowers the resistive loss caused by it, allowing the MEA to reach higher current densities at the same cell voltage and iridium loading, leading to an improved Ir-PD (lever A). Currently, perfluorosulfonic acid (PFSA) membranes are used, with 125 μm thick Nafion® 115 considered as the current industry benchmark in commercial PEMWEs due to its adequate hydrogen crossover properties. Reducing the membrane thickness can lead to higher quantities of H_2 crossover leading to the possible formation of explosive H_2/O_2 mixtures [50], which is exacerbated by both idling/low current density operation and high differential pressure (≥30 bar) operation. Furthermore, a thinner membrane can also shorten the lifetime of the MEA due to mechanical failures from pinhole formation and rupturing, as well as chemical failures due to membrane thinning from radical attack during operation [51]. Therefore, for thin membranes, higher mechanical strength, greater resistance to radical attack and reduced H_2 crossover will be necessary, either by changing the properties of the membrane itself or by additives such as reinforcements, radical scavenging and recombination catalysts [52–57]. However, we see this as an achievable technological advancement, allowing membrane thicknesses to be eventually reduced to ~50 μm. Similarly, Ir-PD can also be reduced by improvements in PTLs and microporous layers, lowering the electronic resistance (R_{el}) during operation [58].

The overpotential due to mass transport resistance ($j_{geo} \cdot R_{mt}$, yellow wedge in Fig. 7) is thought to be primarily due to a pressure build up at the cathode due to the flooding of pores in the CL [47]. The mass transport contribution shown in Table S11 can be minimised by optimisation of the PTLs, the microporous layers and the morphology of the cathode CL. The cathodic kinetic overpotential (η_{kin}^{HER}, green wedge) and the protonic and electronic resistive losses in the cathode CL ($j_{geo} \cdot R_{eff}^{cath}$, red wedge) are minor in comparison to the other overpotentials, as the HER is very facile [44] and the carbon-supported Pt catalyst highly conductive. Indeed, the HER overpotential on Pt/C is typically < 5 mV at a current density of 2 A cm^{-2} and the total contribution of the cathode

Table 5
Ir-PD targets for the optimistic scenario.

	2022	2030	2050
Optimistic Ir-PD target at future E_{cell} (Fig. 2b) / mg_{Ir} W^{-1}	0.43	0.05	0.04
Optimistic Ir-PD normalised to 1.79 V / mg_{Ir} W^{-1}	0.45	0.04	0.01

catalyst is thus < 2% of the total overpotential, in agreement with Bernt and Gasteiger [47].

6. Future pathways toward reduced iridium-specific power density

The likelihood of the optimistic scenario for Ir-PD improvement (see Section 2) being realised using these technological levers can be evaluated by comparison to PEM hydrogen fuel cell technology. Fuel cell technology is at a more advanced stage of development than PEMWE, due to significant research focus since the early 1970s [59]. This, combined with the similarity of the technologies, means that comparing the degree of improvement in platinum-specific power density in fuel cells is a useful indicator of the progress PEMWE technology could make in the coming decades. The platinum-specific power density of fuel cells has reduced from ~3 mg_{Pt} W^{-1} in 1991 [60] to 1.1 mg_{Pt} W^{-1} in 2005 [61,62] and 0.14–0.2 mg_{Pt} W^{-1} today [63,64], *i.e.* just over one order of magnitude reduction over three decades. The magnitude of this improvement is similar to the PEMWE Ir-PD improvement required by the optimistic scenario by 2050, (0.43 mg_{Ir} W^{-1} in 2022 down to 0.04 mg_{Ir} W^{-1} in 2050, as shown in Fig. 2a), offering encouragement that the optimistic scenario can be realised.

Different future technological pathways towards the optimistic scenario's Ir-PD targets were constructed in order to examine the relative importance of levers A, B and C for reducing Ir-PD. Pathways 1–3 were constructed by holding one of the three levers constant with time, while the other two levers were varied such that the optimistic scenario Ir-PD targets (Table 5) were met, as shown in Table 6. Each pathway effectively investigates the relative importance of the lever that is held constant by demonstrating how much the other two levers need to compensate to get the same Ir-PD performance. In a fourth technological pathway, all three levers were varied to investigate their combined effect on Ir-PD.

For simplicity and given that ~67% of R_{cell} is contributed by R_{memb} at 2 A cm^{-2}, R_{memb} was used as a proxy for R_{cell}, *i.e.* R_{memb}, instead of R_{cell}, was held fixed in Pathway 1. To further simplify the model, in Pathways 1 and 4 the OER catalyst level levers of $j_{0,mass}$ and loading were linked as dependent variables by holding their product, $j_{0,geo}$, constant (Table 6). In effect, this means that we are choosing one of an infinite number of pathways for how $j_{0,mass}$ and loading can vary with respect to each other to match the Ir-PD performance targets. While it is impossible to predict which pathway the technology will take in the future, in our opinion the value of the product chosen here showcases realistic pathways.

For each pathway, corresponding MEAs were modelled using Eq. (15). The equivalent analysis for the conservative scenario can be found in the SI.

The starting point for each pathway was a current SoA MEA. The SoA $j_{0,mass}$ value at 80 °C of 1.48 x 10^{-7} A mg_{Ir}^{-1} was extrapolated from the temperature dependent study of exchange current densities completed by Lettenmeier *et al.* [38]. The catalyst used in this study was an amorphous IrO_x catalyst with an iridium metal core, which are known to be highly active towards the OER [48–50]. 125 μm thick Nafion® 115 was used as the SoA membrane. R_{cell} was calculated based on the work of Bernt and Gasteiger [37], as a function of the thicknesses of the membrane and the anode CL, to be 0.131 Ω cm^2 (for details and the calculated R_{cell} values, see Section S5). The SoA loading used is 1.89 mg_{Ir} cm^{-2}, which is in line with multiple industrial reports [2,7,22,26].

In Pathway 1, the membrane thickness, and, therefore, R_{memb}, was held constant. While the loading reduction required to match the 2030 optimistic target is considered to be feasible, hitting the 2050 target would require iridium loading to reduce to 0.06 mg_{Ir} cm^{-2}. As discussed in Section 2, MEAs with very low loadings of iridium will be difficult to reach due to dissolution. In the optimistic scenario, we consider MEAs with relevant lifetimes to be prohibitively difficult to reach below iridium loadings of 0.10 mg_{Ir} cm^{-2} (*cf.* 0.22 mg_{Ir} cm^{-2} for the conservative scenario) due to iridium dissolution. Therefore, the Pathway 1 2050 loading is considered unfeasible. The projected 30x increase in $j_{0,mass}$ by 2050 would also be very challenging: for comparison, while research in hydrogen fuel cell technology has managed to increase the $j_{0,mass}$ of the hydrogen oxidation reaction by a factor of ~ 23 in wet cell testing, so far this has only translated to a ~ 3.5x increase in MEA performance [51], although this may improve in the future with MEA optimisation. This suggests that the projected 30x increase in the $j_{0,mass}$ of IrO_x for the OER in a MEA is unrealistic, barring a step-change in catalyst activity. These difficult targets show that reducing membrane thickness (and therefore R_{memb}) will be crucial to meeting the optimistic scenario's Ir-PD targets.

Pathway 2, where loading was kept constant, produced non-sensical values for $j_{0,mass}$ in 2030 and 2050. This is because in order to match higher j_{mass} values at the same loading, j_{geo} would have to be so high that the resistive term in Eq. (15) becomes unrealistically large.

In Pathway 3, $j_{0,mass}$ was fixed and the membrane thickness reduced from today's 125 μm to 80 and 50 μm by 2030 and 2050, respectively, with 50 μm being the lower limit, as discussed above. This means that the voltage loss at 2 A cm^{-2} due to R_{memb} decreases from 176 mV in 2022 to 113 mV in 2030 and 70 mV in 2050, respectively. We consider these reductions in membrane thickness to be feasible if the improvements discussed in Section 5 can be implemented. In this pathway, reaching the 2030 optimistic Ir-PD target is feasible in terms of loading, but hitting the 2050 target again requires iridium loadings to reduce to below 0.10 mg_{Ir} cm^{-2} by 2050. As discussed above, we consider loadings < 0.1 mg_{Ir} cm^{-2} to be unfeasible. This shows that a reduction in membrane thickness of this scale and realistic reduced loadings alone are unlikely to be sufficient to reach the 2050 optimistic Ir-PD target.

Table 6
Membrane thickness (R_{memb}) (lever A), iridium loading (lever B) and $j_{0,mass}$ (lever C) for MEAs corresponding to the different technological development pathways in the optimistic scenario. Variables that are held constant in each pathway are in *italics and underlined.* For assumptions, see Table 4.

	A) Membrane thickness (*cf.* R_{memb}) / μm[a]			B) Loading / mg_{Ir} cm^{-2}			C) $j_{0,mass}$ x 10^{-7} / A mg_{Ir}^{-1}		
	2022	2030	2050	2022	2030	2050	2022	2030	2050
Cell operating voltage (E_{cell}) / V	1.80	1.75	1.58	1.80	1.75	1.58	1.80	1.75	1.58
Optimistic Ir-PD target / mg_{Ir} W^{-1}	0.43	0.05	0.04	0.43	0.05	0.04	0.43	0.05	0.04
Pathway 1: Fixed membrane (R_{memb})	*125*	*125*	*125*	1.89	0.20	0.06	1.5[b]	14	45
Pathway 2: Fixed loading	125	80	50	*1.89*	*1.89*	*1.89*	1.5[b]	N/A	N/A
Pathway 3: Fixed ($j_{0,mass}$)	125	80	50	1.89	0.23	0.05	*1.5*[b]	*1.5*	*1.5*
Pathway 4: All varied	**125**	**80**	**50**	**1.89**	**0.27**	**0.10**	**1.5**[b]	**10**	**27**

[a] Membrane conductivity assumed to be constant. [b] Extrapolated from [49].

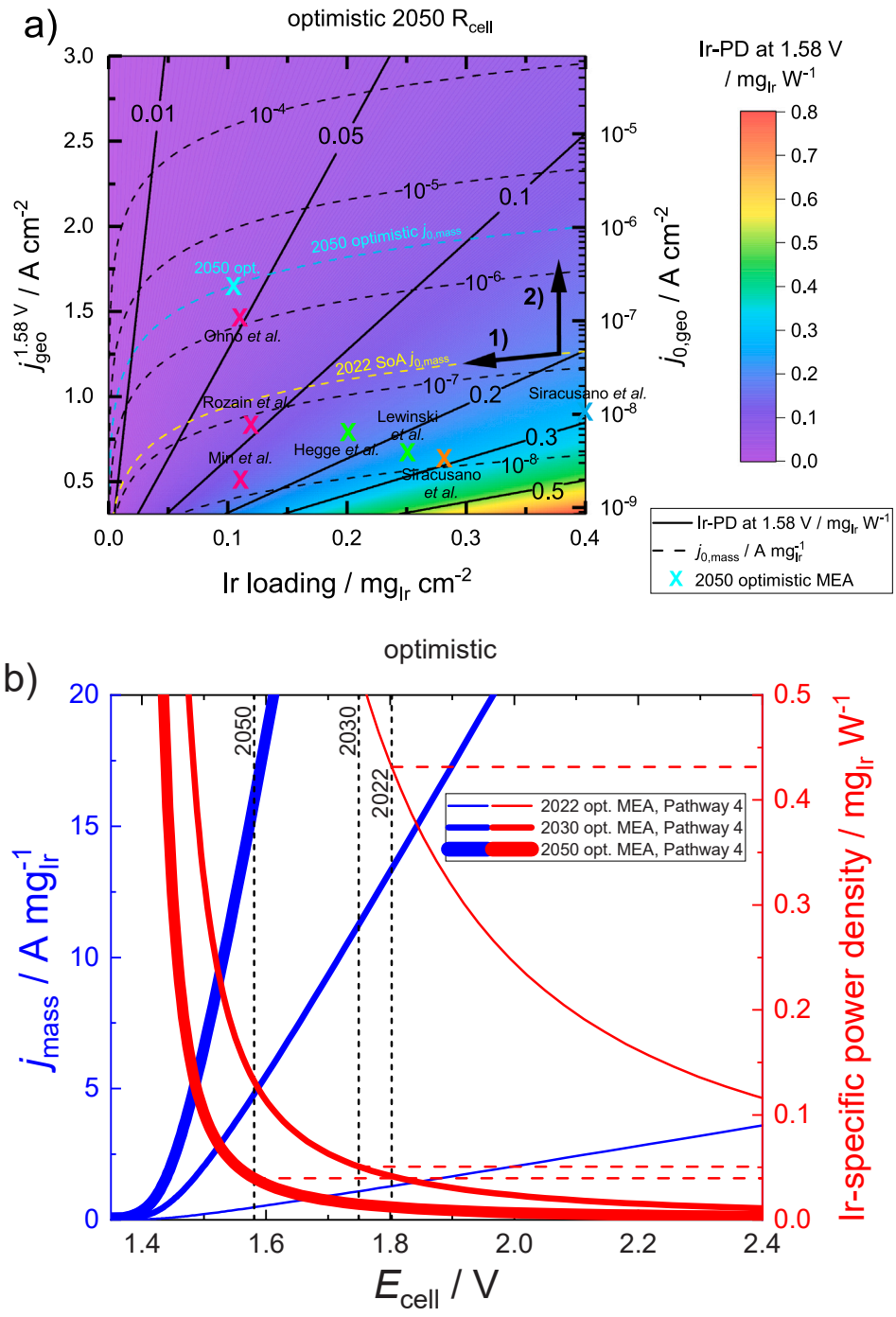

Fig. 8. a) Contour plot of Ir-PD at 1.58 V (solid lines) as a function of geometric current density at 1.58 V ($j_{geo}^{1.58V}$) and iridium loading for MEAs with the 2050 optimistic scenario characteristics, *i.e.* with R_{cell} = 0.065 Ω cm^2 corresponding to 50 μm thick Nafion® 212 and an operating voltage of 1.58 V. Dashed lines indicate constant $j_{0,mass}$. The optimistic scenario Pathway 4 performance is marked by a cyan cross. The best performing literature catalysts in each category and some other notable examples from Section 7 are also marked (light blue cross: nanoparticles, pink crosses: supported catalysts, green crosses: extended surface catalysts, orange cross: mixed oxide catalysts) [34,35,66–70]. Please note these were also normalised to the 2050 membrane (50 μm) using Eq 16 *i.e.,* the current densities marked here may differ to the original datasets in the source publications, which often used membranes with a different thickness. Equations for plotting can be found in Section S7. b) Modelling PEM water electrolyser MEAs meeting the 2022, 2030 and 2050 optimistic Ir-PD performance targets for Pathway 4 (for equivalent analysis of the other pathways and the conservative scenario, see the SI). The iridium loading, mass-specific exchange current density ($j_{0,mass}$) and the membrane thickness (R_{memb}) are variables, as shown in Table 6. Assumptions are shown in Table 4. The thickness of the lines corresponds to how far in the future they are. Note that the scales of the *y* axes are not directly related to each other, as each MEA has a different functional relationship between j_{mass} and Ir-PD.

Therefore, increasing the intrinsic activity of the catalyst will also be necessary.

The fact that, in Pathway 2, where loading was fixed, not even the 2030 Ir-PD performance can be met with today's loadings shows that, within the boundary conditions of the model, lever B (reducing iridium loading) is more effective in lowering Ir-PD than levers A (reducing R_{memb}) and C (increasing $j_{0,mass}$), especially in the short term. The relative impacts of levers B and C on Ir-PD are shown graphically in Fig. 8a, where the Ir-PDs (contour lines) of MEAs are shown as a function of the iridium loading (*x* axis) and $j_{0,mass}$ (dashed lines), for a fixed R_{cell} corresponding to a 50 μm membrane. Ir-PD can be reduced by 1) travelling along the diagonal arrow, *i.e.* decreasing the iridium loading at a fixed $j_{0,mass}$ (lever B) and by 2) travelling along the vertical arrow, *i.e.* increasing $j_{0,mass}$ at a fixed iridium loading (lever C). The effectiveness of reducing loading is shown by the fact that a 0.10 mg$_{Ir}$ cm^{-2} MEA with today's SoA $j_{0,mass}$ (yellow dashed line) can reach an Ir-PD as low as 0.07 mg$_{Ir}$ W^{-1} at 1.58 V (≈ 0.02 mg$_{Ir}$ W^{-1} at 1.79 V), which is below the 2030 target at

Table 7
The characteristics of the modelled MEAs for the optimistic Pathway 4 scenario.

Optimistic Pathway 4 MEA characteristics	Membrane thickness (R_{memb}) / μm	Loading / mg$_{Ir}$ cm^{-2}	$j_{0,mass}$ x 10^{-7} / A mg$_{Ir}^{-1}$	E_{cell} at 2 A cm^{-2} / V
2022	125	1.89	1.5	1.74
2030	80	0.27	10	1.65
2050	50	0.10	27	1.61

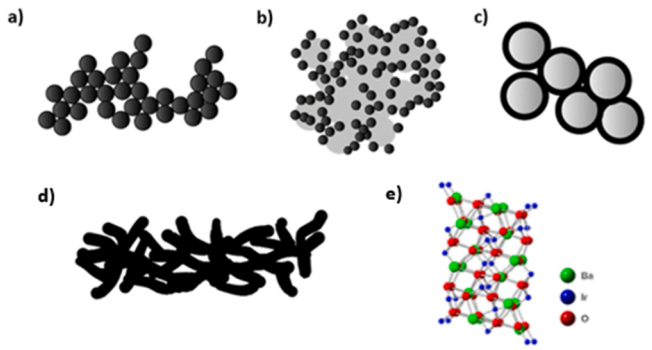

Fig. 9. Schematics illustrating the various iridium-based OER catalyst strategies: a) nanoparticulate; b) supported nanoparticulate; c) core-shell structure; d) extended surface structure; e) mixed oxide.

1.79 V (Table 5). However, while reducing loading is the most effective lever, increasing $j_{0,mass}$ (and reducing membrane thickness) will still be necessary to hit the optimistic 2050 Ir-PD target with loadings $\geq$ 0.10 mg_{Ir} cm^{-2}.

Indeed, the combined effect of using all three levers simultaneously in Pathway 4 is that a loading reduction to 0.10 mg_{Ir} cm^{-2} is sufficient to reach the 2050 optimistic Ir-PD target, as shown by the cyan cross in Fig. 8a. This loading value is more reasonable than the loadings in Pathways 1 and 3, because it is at the 0.10 mg_{Ir} cm^{-2} threshold discussed above and is therefore considered to be achievable with strong technological advancement in terms of dissolution. Additionally, $j_{0,mass}$ only needs to improve by a factor of 18, rather than 30 as in Pathway 1, where R_{memb} was fixed. The deconvoluted overpotentials for Pathway 4 are shown in Fig. 7 (2022) and in the SI (2030 and 2050). It is important to note that although the iridium loading is higher in Pathway 4 compared to Pathways 1 and 3, the usage of iridium per kg of hydrogen produced is fixed from Fig. 2 to be exactly the same at each future timepoint for all four pathways.

A caveat is that an early step-change in the membrane thickness or conductivity could significantly alter this picture. For example, Hystar AS's PEMWE technology looks to avoid the formation of explosive H_2/O_2 mixtures by diluting the crossover hydrogen with air on the anodic side of the MEA. While this does not address any inherent mechanical strength or degradation issues in the membrane, it is claimed to enable the use of a 20 μm thick PFSA membrane [65], which would allow the iridium loading to be as high as 0.51 mg_{Ir} cm^{-2} rather than 0.27 mg_{Ir} cm^{-2} for Pathway 4 in the 2030 optimistic scenario. Additionally, the development of hydrocarbon membranes could also significantly reduce R_{memb} due to increased membrane conductivity [142]. Such improvements in membrane technology could ease the pressure to develop more active catalysts and CLs with lower loadings, shifting the research focus more towards improving MEA durability.

In Fig. 8b, model MEA performances corresponding to the optimistic Pathway 4 scenario were plotted using Eq. (15), with Table 7 summarising the practical parameters of these MEAs for experimentalists to compare their results against. The mass-specific polarisation curves (blue lines) illustrate the scale of the challenge to reduce Ir-PD. In the optimistic scenario, the iridium mass activity produced by an electrolyser at 1.79 V will have to increase from today's 1.2 A mg_{Ir}^{-1} to 13 A mg_{Ir}^{-1} by 2030 and 44 A mg_{Ir}^{-1} by 2050 (all normalised to 1.79 V = 70% LHV efficiency for comparability as mentioned in Section 5, see Table S16), all while maintaining equivalent operational lifespan. The red lines in Fig. 8b also show how the corresponding Ir-PD of each MEA changes with E_{cell}.

Fig. 8b can be used to discuss the likely operating voltage of electrolysers in the future. E_{cell} (horizontal axis) may be thought of as part of a PEMWE plant's operational expenditure (OpEx), as the cell voltage is proportional to electricity usage. The Ir-PD (right-hand axis) can be thought of as the iridium-dependent portion of a plant's capital expenditure (CapEx), as a lower Ir-PD means less iridium used in MEAs to make hydrogen over the MEA's lifetime. To minimise OpEx, operating voltage should be reduced by moving to the left along the red lines in Fig. 8b, while to minimise CapEx and avoid iridium supply constraints, Ir-PD should be minimised by moving to the right along the red lines. The most cost-effective balance of these opposing cost drivers will help determine the ideal operating voltage of a PEMWE plant.

Fig. 2b shows how governmental/intergovernmental organisations currently expect operating voltage to change with time. Given that electricity cost is projected to account for 70–90% of the cost of green hydrogen in the long term [71], it is likely that plants will balance

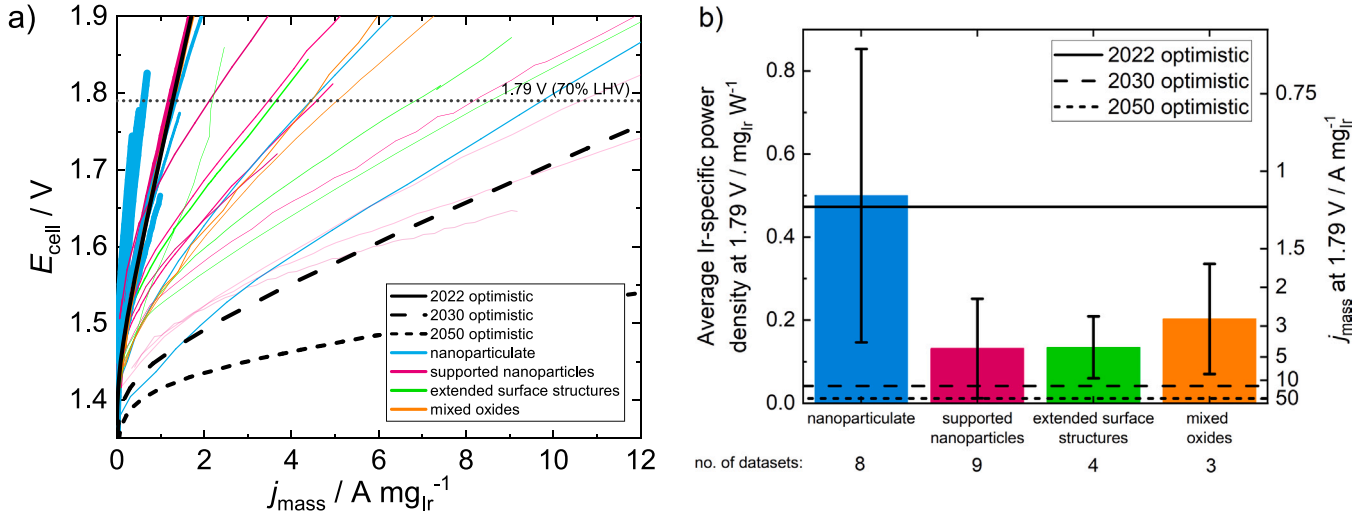

Fig. 10. PEMWE MEA performance at 80 °C and atmospheric pressure of various iridium-based OER catalysts gathered from the literature [34,35,49,66–70,72,73,77,82,84,97,99–101]. a) Polarisation curves were obtained by iR-correcting the test data using the Ohmic resistance value given within the corresponding reference and then applying a uniform R_{cell} of 0.131 Ω cm^2 (Nafion® 115) to make the datasets comparable (see Eq. 16). Line thickness is representative of the iridium loading, which ranges 0.11 – 2.5 mg_{Ir} cm^{-2}. The black lines represent model MEA performances for the optimistic scenario with a fixed Nafion® 115 membrane (Pathway 1 in Table 6). b) The average Ir-PD of the catalyst strategies evaluated based on the literature datasets. The black lines show the optimistic scenario target Ir-PDs normalised to 1.79 V (Table 5). The j_{mass} values of the black lines correspond to the intersection points of the black polarisation curves with the 1.79 V line in a).

between runing at the minimum voltage possible while still allowing Ir-PD to be high enough to avoid the expansion of the PEMWE market becoming limited by iridium supply. On the other hand, in a future where renewable electricity becomes more abundant and cheaper than expected (*i.e.* significantly less than 60 € MWh^{-1} in 2050 in the EU [71]), electrolysers could be run at higher voltages to further reduce Ir-PD.

7. Review of iridium-based catalyst strategies

To reach the optimistic Ir-PD targets using the catalyst focused levers B and C discussed above while being industrially relevant, an IrO_x catalyst used in a MEA will have to fulfil some key requirements:

- high intrinsic iridium mass activity (optimistic 2022–2050 $j_{0,mass}$: 1.5–27 x 10^{-7} A mg_{Ir}^{-1}, see Table 6);
- good stability against iridium dissolution and other degradation mechanisms (optimistic dissolution rate: < 2.0 x 10^{-6} mg_{Ir} cm^{-2} h^{-1} by 2050 (calculation in Section S2.5));
- the ability to form uniform CLs with reasonable laterally conductive at loadings < 0.3-0.5 mg_{Ir} cm^{-2} to enable high catalyst utilisation within the layer [27,42,76]
- synthetic method readily scalable for manufacture.

There are various catalyst strategies that can be used to improve the Ir-PD of PEMWEs using the catalyst focused levers B and C (illustrations in Fig. 9):

- Nanoparticulate: pure iridium or iridium oxide nanoparticles [49,68, 72–76]
- Supported nanoparticulate: iridium or iridium oxide nanoparticles on metal oxide support [34,35,70,77–83]
- Core-shell structures: iridium or iridium oxide shell around a core of a different composition [84–87]
- Extended surface structures: iridium or iridium oxide catalysts with continuously connected surface areas [67,88–94]
- Mixed oxides: mixed oxide of iridium and other elements, including where the other elements cause structure changes, for example perovskites, pyrochlores and hollandites [69,73,95–98]

To compare the current SoA performance of these different catalyst strategies, a large set of mass-specific polarisation curves tested at equivalent temperature and pressure (80 °C and atmospheric pressure, see Table S17) were collected from the literature. Note that for the purposes of this review, core-shell catalysts were categorised as supported catalysts. The datasets were normalised by first subtracting the reported Ohmic resistance to give Ohmic resistance-free MEA testing data (j_{geo} *vs* $E_{iR-free}$). Then, a consistent cell resistance corresponding to a current SoA MEA (*i.e.* with R_{cell} = 0.131 Ω cm^{-2} for 125 μm thick Nafion® 115, see Table S14) was added according to Eq. (16), allowing the literature testing data to be compared to each other as if they were effectively tested in the same electrolyser, as shown in Fig. 10a. While we realise the running conditions (*e.g.* water flow rate, clamping pressure, *etc.*) and cell design (*e.g.* flow field plate, PTL type, *etc.*) can have an effect on the testing, it was felt this was as close to a like to like comparison as possible. Nafion® 115 was chosen as it is the current industry standard in terms of durability and performance.

$$E_{cell} = E_{iR-free} + j_{geo} \cdot R_{cell} \quad (16)$$

The line thickness in Fig. 10a was adjusted according to the iridium loading in the respective MEAs. The black lines show model MEA polarisation curves corresponding to the optimistic MEAs in Pathway 1, see Fig. S14b. Pathway 1 was used because the fixed membrane thickness (Nafion® 115) allows comparison with the literature catalysts.

The fact that the light blue lines which corresponding to nanoparticulate catalysts are generally thicker shows that these catalysts are used at higher iridium loadings, and therefore fail to advance much beyond the 2022 optimistic performance (solid black line in Fig. 10). This is because these catalysts have a high iridium volume density, leading to the formation of disconnected 'islands' in the CL below a loading of ~0.3-0.5 mg_{Ir} cm^{-2}, where the catalyst is effectively electronically isolated from the rest of the layer [27,42,76]. The inability of nanoparticulate catalysts to form conductive CLs with loadings < 0.3-0.5 mg_{Ir} cm^{-2} limits their ability to use the lever of lower loadings to improve the Ir-PD of PEMWEs. This effect means that to achieve the Ir-PD targets going forward, nanoparticulate catalysts need to significantly improve their $j_{0,mass}$. Developments in this direction include 1) very high surface area catalysts, leading to a highly active catalyst that can get close to the 2030 optimistic scenario Ir-PD (*e.g.* Adams fusion IrO_2, [68]) and 2) catalysts with higher surface area-specific OER activity, for example by having a hydrated iridium oxide surface (Alfa Aesar Premion (AA), [84]).

On the other hand, supported nanoparticulate catalysts (pink in Fig. 10) have demonstrated lower Ir-PDs compared to nanoparticulate catalysts, with some testing performances even surpassing the 2030 optimistic target of 0.04 mg W^{-1} at 1.79 V (Table 5) [34,35,70]. The primary effect here is likely to be the lowered iridium volume density of the catalyst, as the supporting metal oxide effectively disperses the IrO_x nanoparticles. This means that for the same amount of iridium, a thicker CL will be formed, resulting in homogeneous and conductive CLs with loadings as low as 0.11 mg_{Ir} cm^{-2} having been demonstrated [34,70]. A secondary effect is that supporting IrO_x nanoparticles on a high surface area metal oxide maximises the number of surface iridium sites available for catalysing the OER, therefore increasing $j_{0,mass}$. A further advantage may be the so-called catalyst-support interaction, where the electronic interaction with the metal oxide support also increases $j_{0,mass}$ [78,102, 103].

A note of caution on supported catalysts, however, is that the nature of the supporting material imposes its own limitations. Non-conductive supports such as TiO_2 are demonstrated to be stable under PEMWE conditions [35]. However, the conductivity of the catalyst drops off below an iridium content corresponding to the percolation threshold (where conduction pathways are no longer possible), which Oakton *et al.* [104] found to be around 40 mol% (65 wt%) for their particular catalyst. Therefore, non-conductive supports are limited in the reduction in iridium loading they are able to achieve. Furthermore, using electrocatalysts containing TiO_2 has been shown to lead to degradation of the PEM in fuel cells through a Fenton reaction [105], casting doubt on its suitability as a viable catalyst support in PEMWE. Conductive supports, such as doped tin oxides, can form conductive CLs with significantly lower iridium loadings [34,70,81,82]. However, their stability under PEMWE is unproven and the work of Geiger *et al.* [106] has shown that dissolution of the dopants can lead to a loss in conductivity over time. Therefore, while supported nanoparticulate catalysts have the potential to reach very impressive Ir-PDs, further work is necessary to prove their stability or to find conductive support materials which are more stable.

Iridium-based extended surface structures (*e.g.* nanorods, nanowires, thin films *etc.*, green in Fig. 10) are able to get close to the 2030 optimistic target. Fewer oxide-oxide interparticle interactions due to the continuous connectivity of the catalyst surface in two dimensions lead to CLs that retain a high layer conductivity even at loadings as low as 0.2 mg_{Ir} cm^{-2} [66,67]. These materials can be made *via* physical vapour deposition [88,92], atomic layer deposition [83], de-alloying [91–93], spin coating [16,107] and more conventional wet-chemistry synthetic methods [78]. A notable commercial example is the 3M nanostructured thin film (NSTF), where a continuous layer of iridium is deposited onto whiskers of an organic crystal [66,88]. However, these materials are often composed of metallic iridium or amorphous IrO_x, which have been shown to be significantly less stable towards dissolution in wet cell testing than crystalline IrO_2 [31,108–110]. On the other hand, the 3M NSTF material has shown negligible performance loss over 5000 h in MEA testing at 2 A cm^{-2} [88]. Further work is necessary to investigate the stability of extended surface structures in MEA testing.

Mixed iridium oxides (orange in Fig. 10) can improve the Ir-PD by thrifting iridium. Alloying iridium with ruthenium results in the formation of a ruthenium-rich core, iridium-rich shell structure during operation, due to the preferential dissolution of ruthenium from the surface [111,112]. These catalysts have promising performance, as they effectively replace the core of the iridium nanoparticles with significantly cheaper, but still relatively stable ruthenium [69,73,113,114]. Until the ruthenium has leached from the surface, it also contributes an activity benefit, as it is more active than iridium for the OER. Other alloying options working on a similar principle are tin and nickel [86, 97].

Mixed oxides can also improve Ir-PD by increasing the intrinsic OER activity of the catalyst. For example, Sun *et al.* [115,116] found that the beneficial shifting of electronic energy levels, brought about due to distortion of the IrO_6 octahedra in various mixed oxides, increased the fundamental activity of these materials. Similarly, Willinger *et al.* [117] showed that hollandite-like $K_{0.25}IrO_2$ mixed oxides had improved intrinsic activity, which they attributed to the presence of more edge-sharing IrO_6 octahedra. Various iridium-based perovskite structures have also been shown to have significantly improved activity [95, 118,119].

While some mixed oxide catalysts have shown promising intrinsic activities at wet cell level [95,96,115–118], there are limited reports with MEA level testing available, with the exception of iridium-ruthenium catalysts, which are well documented. This may imply that mixed oxides often have stability issues and further research would be beneficial to understand their potential.

Given that high iridium recycling rates from EoL MEAs will be crucial to avoid a scenario where the growth of the PEMWE market is limited by iridium supply, it is important to 'design-to-recycle' when developing novel catalysts. For example, when developing supported or mixed oxide catalysts, the extra recycling cost incurred by introducing elements additional to iridium should be balanced against their performance improvement. The extra cost is the result of needing to separate the additional elements from the iridium in the recycling phase.

The effectiveness of these four catalyst strategies in reducing Ir-PD is shown in Fig. 10b, where the average Ir-PD of each strategy at 1.79 V is plotted. When the test data for a catalyst did not reach 1.79 V, an extrapolation of the linear section of the polarisation curve was performed to deduce Ir-PD at 1.79 V. To aid comparison, the optimistic Ir-PD targets were normalised to 1.79 V (see discussion in Section 5) using the Pathway 4 polarisation curves in Fig. 8b (see Table 5). Based on the literature data, the effectiveness of the different strategies in reducing Ir-PD was found to be in order of supported nanoparticles ≈ extended surface structures > mixed oxides > nanoparticles, although it should be noted that the large standard deviations in the literature datasets mean there is a possibility for these to reorder. A more detailed discussion, including a stability aspect, is given in the next section.

While so far this review has considered the differences between catalyst strategies, significant improvements in Ir-PD can be achieved by optimising the anode CL without altering the nature of the catalyst itself. Optimising the CL can lower Ir-PD both through improving the structure of the CL itself (*e.g.* lower R_{eff}^{an} due to optimised porosity), and by lowering the threshold loading below which poor quality CLs are formed. This effect can be illustrated by considering the AA catalyst. Van Pham *et al.* [84] tested an AA MEA with a loading of 1.2 mg_{Ir} cm^{-2}, achieving a power density of 0.42 mg_{Ir} W^{-1} at 1.79 V (Table S17). In comparison, Su *et al.* [100] found that they were able to lower the loading to 0.38 mg_{Ir} cm^{-2} through optimisation the CL and the use of a novel coating method, achieving a power density of 0.06 mgIr cm-2 at 1.79 V. Despite using the same commercial anode catalyst, the Ir-PD was improved by an order of magnitude to close to the 2030 optimistic target. The bulk of this improvement can be attributed to the lower iridium loading enabled by the more optimised CL structure. Su *et al.* [100] claimed that a high interfacial contact between the membrane and the CL, along with the uniformly porous structure of the CL, were responsible for the improved performance.

The fact that Fig. 10 features some catalysts that are already hitting the optimistic scenario's 2030 Ir-PD target suggests that the catalyst activities and loadings necessary for the optimistic scenario will be technologically feasible, even if, as discussed in the next section, achieving the required catalyst lifetimes will be challenging. This offers encouragement that the optimistic scenario can be realised. Some of the best performing literature catalysts from Fig. 10 were plotted in Fig. 8a to show their positions in the $j_{0,mass}$ and iridium loading parameter space.

8. Future outlook and catalyst degradation

Given that in Section 6 it was found that reducing the MEA iridium loading is the most effective lever for lowering Ir-PD within the boundary conditions of the model, in our opinion more research should be focussed on developing catalysts that can be formulated into homogeneous and conductive CLs even at very low loadings. As discussed above, this requires catalysts with lower iridium volume densities or extended surface structures, so that conduction networks in the CL are retained even at loadings < 0.3-0.5 mg_{Ir} cm^{-2}. To gauge this development strand, it would be helpful if the iridium volume density of novel catalyst materials were reported, as done by Bernt and Gasteiger [42].

Alongside iridium volume density, performance stability also requires greater focus when designing novel catalysts, especially since lower loadings can lead to faster performance degradation [32,120], as a larger fraction of iridium sites are lost at an equivalent rate of iridium dissolution. Performance loss over the course of MEA degradation testing should be provided alongside activity measurements as standard, and compared to the DoE's 2030 target of 1.6 μV h^{-1} at 3 A cm^{-2} [28]. Degradation testing can be performed either *via* constant voltage or current holds, or *via* accelerated stability testing (AST) using a fluctuating voltage profile [69,121–125]. Constant hold degradation testing should be > 1000 h to allow for meaningful long-term stability data to be gathered beyond the initial ~100 h needed to condition the MEA [69] and to allow for the performance to stabilise [43]. Alternatively, a suitable AST needs to be developed. However, work is still needed to verify whether ASTs are measuring the degradation mechanisms that occur in the real system, rather than accelerating degradation mechanisms that are unlikely to occur under standard operation. Alongside electrochemical degradation testing, iridium dissolution and migration observations made using a number of *in situ* and *post mortem* analytical techniques can help deduce the performance loss due specifically to the anode catalyst [32,33,126–129], and should be compared to the iridium dissolution rate of < 2.0 x 10^{-6} mg_{Ir} cm^{-2} h^{-1}, as stated in Section 7. This is important because performance loss in MEAs can occur for several different reasons [19].

Wet-cell (*e.g.* flow cells, gas diffusion electrode cells and the rotating disk electrode) testing is useful for assessing the activity and stability of novel catalyst materials where access to MEA testing is not available, or if catalysts were produced in smaller quantities than needed for MEA testing. Iridium dissolution can be screened *via ex situ* inductively coupled plasma mass spectrometry (ICP-MS), while in-depth understanding of the dissolution mechanism can be gained by coupling to techniques *in situ*, such as ICP-MS [108,109,130] and electrochemical quartz crystal microbalance [128,131]. Care must be taken on how catalyst degradation in wet-cell testing is related to degradation in MEA testing, since it has been shown that the two are not directly relatable due to a harsher operating environment and bubble formation in the wet-cell [132–134]. However, some studies are starting to align the trends between the two techniques [133–135], and we believe wet-cell degradation testing still has a place in the field as a complementary technique. Nonetheless, novel catalysts should be tested at the MEA level at an early stage to ensure they fit the other criteria, such as processability into a conductive CL.

It would be helpful if these degradation testing techniques were organised into standardised degradation testing protocols, similarly to

the DoE protocols for fuel cells [136,137]. The current lack of standardisation is exemplified by the catalysts discussed in Section 7. While most of the datasets in Fig. 10 were reported alongside degradation testing data (Table S17), these degradation tests were often run at different current densities, making comparison of degradation difficult. Furthermore, most of the degradation tests were well under 1000 h, making it difficult to reliably estimate their rate of performance loss [43]. Also, the degradation tests were carried out on MEAs with different loadings, which affects their degradation rates. Therefore, while Fig. 10 provides a good overview of the activity of these catalysts, further standardised degradation testing would be necessary to compare them on the grounds of stability and assess their viability for industrial use.

Although the fact that Fig. 10 features some catalysts that are already hitting the optimistic scenario's 2030 Ir-PD target is encouraging, the CLs made from these catalysts must sustain a similar level of activity over the MEA's lifetime, which will be a significant research challenge given that lower loading CLs tend to degrade more rapidly due to iridium dissolution [32]. As discussed in Section 2, the current minimum iridium loading necessary to avoid complete dissolution of an amorphous IrO_x CL over a 10-year operational lifetime was estimated as 0.65 mg_{Ir} cm^{-2}, based on an electron microscopy study of the MEA after degradation testing (see Section S3.5) [33]. This means that if catalyst stability cannot be significantly improved, the loadings on the order of 0.1 mg_{Ir} cm^{-2} necessary to reach the optimistic Ir-PD targets would not be possible. This is underlined by the fact that only a few of the catalysts in Fig. 10 have degradation rates below 10 μV h^{-1}, as shown in Table S17 (*cf.* DoE 2030 target of 1.6 μV h^{-1}). On the other hand, Lewinski *et al.* [88] and Gasteiger *et al.* [43] have demonstrated SoA MEAs with loadings of 0.25 mg_{Ir} cm^{-2} showing performance loss within the DoE target over > 3000 h of testing, demonstrating the possibility of developing very low loading MEAs with sufficient stability at the laboratory scale. Nonetheless, in our opinion greater focus should be placed on leveraging the growing understanding of iridium dissolution mechanisms [18,108,109,138–141] to develop catalysts that are more stable towards dissolution.

Care must be taken when evaluating synthesis methods for industrial use, as many methods are not readily scalable for manufacture, *e.g.* electrochemical leaching. Ideally, a synthesis would avoid highly dilute solutions and reaction times longer than a few hours.

9. Conclusions

The present study investigates the Ir-PD targets that must be achieved in the future to avoid a situation where PEMWE capacity is limited by iridium supply, models the future iridium demand of the PEMWE sector and reviews the ability of different catalyst development strategies to reach the Ir-PD targets.

A review of the Ir-PD targets put forward by governmental/intergovernmental organisations and the academic literature was used to model a conservative and an optimistic scenario of technological progress in terms of Ir-PD, reaching 0.10 and 0.04 mg_{Ir} W^{-1}, respectively, by 2050. The conservative scenario was limited to 0.10 mg_{Ir} W^{-1} to take into account that there might always be a certain amount of iridium dissolution that prevents loadings less than ~0.2 mg_{Ir} cm^{-2} being used.

For each of these technological development scenarios, the annual iridium demand of the PEMWE sector was calculated for capacity growth trajectories based on the IEA APS, IEA NZE and Hydrogen Council projections, respectively. The recycling rate was assumed to increase linearly from 70% in 2020 to the theoretical maximum recycling rate of 100% by 2035, although sensitivity studies for recycling rate and other assumptions were provided.

For the IEA APS in the conservative scenario, the annual primary iridium demand of the PEMWE sector would be over 20% of global annual primary supply up to 2032. We consider 20% of annual global supply (1.5 t yr^{-1}) to be a realistic and feasible portion of the primary iridium market for the PEMWE sector to command. Therefore, in the APS's conservative scenario, the roll-out of PEMWE capacity would likely be limited by primary iridium supply.

On the other hand, in the optimistic scenario of technological progress, the primary iridium demand of the IEA APS capacity growth would remain below the threshold of 20% of annual primary supply through to 2050, and therefore would not be constrained by iridium supply. Indeed, in this scenario the PEMWE sector would require only 9% of cumulative global primary iridium supply up to 2050.

In the conservative scenario, the IEA NZE capacity growth projection would require improbable quantities of iridium up to 2037, and is therefore considered to be unrealistic. In the optimistic scenario, however, while iridium demand would still breach the 20% threshold for a period of 10 years, only 16% of cumulative global primary iridium supply is required up to 2050. Therefore, if the initial surge in primary iridium demand could be absorbed by the market, the IEA NZE would be attainable with the optimistic technological development scenario and very high recycling rates.

The PEMWE capacities that could be reached if a given portion of global primary iridium supply was available to the sector each year were also modelled. With the realistic constraint of 20% of iridium supply applied and again assuming that the recycling rate rises linearly from 70% in 2020 to 100% in 2035, the global installed PEMWE capacity would reach ~470 GW by 2050 in the conservative scenario, and ~1.3 TW by 2050 in the optimistic scenario. Compared to a scenario with no iridium recycling, this represents a ~2.7x increase in capacity, demonstrating the importance of implementing high iridium recycling rates from EoL MEAs. That being said, the development of a large-scale PEMWE industry is not predicated on iridium recycling, as in the optimistic technological development scenario the IEA APS 2050 target capacity can almost be reached with no recycling assumed.

The key technological levers for enabling PEMWE expansion free of iridium supply constraints are increasing the intrinsic OER activity of the catalyst ($j_{0,mass}$), decreasing iridium loading (L_{Ir}) in MEAs and reducing the thickness of the PEM (reducing R_{memb}). Modelling of future MEA performances found the effectiveness of these levers in lowering Ir-PD to be in the order of decreasing catalyst loading > increasing $j_{0,mass}$ ≈ decreasing R_{memb} through thinner membranes. A target 2050 MEA was also put forward, with a loading of 0.1 mg_{Ir} cm^{-2}, OER catalyst $j_{0,mass}$ of 3 x 10^{-6} A mg_{Ir}^{-1} and a 50 μm PFSA membrane.

A literature review comprising MEA testing of the different iridium-based OER catalyst strategies found their effectiveness in reducing Ir-PD to be in the order of supported nanoparticles ≈ extended surface structures > mixed oxides > nanoparticles. Indeed, it was shown that supported nanoparticulate and extended surface structure catalysts are already able to achieve MEA performances corresponding to the optimistic scenario's 2030 target, although the stability of their performance requires further investigation. Future catalysts should have a lower iridium-specific volume density and high conductivity, allowing them to form homogeneous and conductive CLs even at loadings < 0.3-0.5 mg_{Ir} cm^{-2}. Significant further work is needed to improve catalyst stability towards dissolution to enable MEAs with industrially relevant lifetimes to be developed.

Although the optimistic scenario of Ir-PD reduction is highly challenging, based on the literature MEA performances reviewed and the fact that the degree of improvement in PGM utilisation necessary in PEMWE has already been achieved in PEM fuel cells over a similar timeframe, in our opinion it is feasible. This means that, if high recycling rates are implemented, global PEMWE capacity could reach up to ~130 GW by 2030 and ~1.3 TW by 2050 using only 20% of global annual iridium supply.

CRediT authorship contribution statement

Mark Clapp: Conceptualization, Methodology, Software, Formal analysis, Investigation, Writing – original draft, Writing – review & editing, Visualization, **Chris Zalitis:** Conceptualization, Methodology, Software, Investigation, Writing – review & editing, **Margery Ryan:** Methodology, Validation, Writing – review & editing.

Declaration of Competing Interest

The authors declare that they have no known competing financial interests or personal relationships that could have appeared to influence the work reported in this paper.

Data Availability

Some of the data is confidential, but some will be possible to be shared on request.

Appendix A. Supporting information

Supplementary data associated with this article can be found in the online version at doi:10.1016/j.cattod.2023.114140.

References

[1] Hydrogen Council, McKinsey & Company, Hydrogen for Net-Zero: A critical cost-competitive energy vector, 2021. https://hydrogencouncil.com/wp-content/uploads/2021/11/Hydrogen-for-Net-Zero.pdf.

[2] T. Smolinka, N. Wiebe, P. Sterchele, A. Palzer, F. Lehner, M. Jansen, K. Steffen, R. Miehe, S. Wahren, F. Zimmermann, Industrialisierung der Wasser elektrolyse in Deutschland: chancen und Herausforderungen für nachhaltigen Wasserstoff für Verkehr, Strom und Wärme (2018). ⟨https://www.ipa.fraunhofer.de/content/dam/ipa/de/documents/Publikationen/Studien/Studie-IndWEDe.pdf⟩.

[3] S. Kiemel, T. Smolinka, F. Lehner, J. Full, A. Sauer, R. Miehe, Critical materials for water electrolysers at the example of the energy transition in Germany, Int. J. Energy Res. 45 (2021) 9914–9935, https://doi.org/10.1002/er.6487.

[4] International Energy Agency, Global Hydrogen Review 2022, 2022. https://doi.org/10.1787/39351842-en.

[5] International Energy Agency, World Energy Outlook 2022, 2022. https://www.iea.org/reports/world-energy-outlook-2022.

[6] International Energy Agency, Net Zero by 2050: A Roadmap for the Global Energy Sector, 2021. https://iea.blob.core.windows.net/assets/deebef5d-0c34–4539-9d0c-10b13d840027/NetZeroby2050-ARoadmapfortheGlobalEnergySector_CORR.pdf.

[7] E. Taibi, H. Blanco, R. Miranda, M. Carmo, IRENA: Green Hydrogen Cost Reduction: Scaling up Electrolysers to Meet the 1.5^{0}C Climate Goal, 2020. https://irena.org/-/media/Files/IRENA/Agency/Publication/2020/Dec/IRENA_Green_hydrogen_cost_2020.pdf.

[8] S. Cherevko, S. Geiger, O. Kasian, N. Kulyk, J.P. Grote, A. Savan, B.R. Shrestha, S. Merzlikin, B. Breitbach, A. Ludwig, K.J.J. Mayrhofer, Oxygen and hydrogen evolution reactions on Ru, RuO2, Ir, and IrO2 thin film electrodes in acidic and alkaline electrolytes: a comparative study on activity and stability, Catal. Today 262 (2016) 170–180, https://doi.org/10.1016/j.cattod.2015.08.014.

[9] A. Cowley, J. Jiang, B. Tang, A. Wang, L. Bloxham, S. Brown, L. Cole, M. Fujita, N. Girardot, R. Raithatha, M. Ryan, Johnson Matthey PGM market report May 2022, 2022. https://matthey.com/documents/161599/509428/PGM-market-report-May-2022.pdf/542bcada-f4ac-a673–5f95-ad1bbfca5106?t=1655877358676.

[10] F. Marscheider-Weidemann, S. Langkau, E. Eberling, L. Erdmann, M. Haendel, M. Krail, A. Loibl, C. Neef, M. Neuwirth, L. Rostek, S. Shirinzadeh, D. Stijepic, L. Tercero Espinoza, S.-J. Baur, M. Billaud, O. Deubzer, F. Maisel, M. Marwede, J. Rückschloss, M. Tippner, Rohstoffe für Zukunftstechnologien 2021 Auftragsstudie – DERA Rohstoffinformationen, 2021. https://www.deutsche-rohstoffagentur.de/DE/Gemeinsames/Produkte/Downloads/DERA_Rohstoffinformationen/rohstoffinformationen-50.pdf;jsessionid=6950C958D62239ED5488B54164FB4195.1_cid321?_blob=publicationFile&v=3.

[11] E. Kriegler, B.C. O'Neill, S. Hallegatte, T. Kram, R.J. Lempert, R.H. Moss, T. Wilbanks, The need for and use of socio-economic scenarios for climate change analysis: a new approach based on shared socio-economic pathways, Glob. Environ. Chang. 22 (2012) 807–822, https://doi.org/10.1016/j.gloenvcha.2012.05.005.

[12] S. Wieclawska, A. Gavrilova, Towards a Green Future. Part 1: How raw material scarcity can hinder our ambitions for green hydrogen and the energy transition as a whole, 2021. https://www.tno.nl/en/newsroom/2021/06/shortage-materials-threatens-green/.

[13] A. Gavrilova, S. Wieclawska, Towards a green future. Part 2: How can we prevent material scarcity and turn our green hydrogen ambitions into reality, 2021. https://www.tno.nl/en/newsroom/2021/06/shortage-materials-threatens-green/.

[14] C. Minke, M. Suermann, B. Bensmann, R. Hanke-Rauschenbach, Is iridium demand a potential bottleneck in the realization of large-scale PEM water electrolysis? Int. J. Hydrog. Energy 46 (2021) 23581–23590, https://doi.org/10.1016/j.ijhydene.2021.04.174.

[15] M. Chatenet, B.G. Pollet, D.R. Dekel, F. Dionigi, J. Deseure, P. Millet, R.D. Braatz, M.Z. Bazant, M. Eikerling, I. Staffell, P. Balcombe, Y. Shao-Horn, H. Schäfer, Water electrolysis: from textbook knowledge to the latest scientific strategies and industrial developments, Chem. Soc. Rev. 51 (2022) 4583–4762, https://doi.org/10.1039/d0cs01079k.

[16] T. Reier, H.N. Nong, D. Teschner, R. Schlögl, P. Strasser, Electrocatalytic oxygen evolution reaction in acidic environments – reaction mechanisms and catalysts, Adv. Energy Mater. 7 (2017), https://doi.org/10.1002/aenm.201601275.

[17] C. Wang, F. Lan, Z. He, X. Xie, Y. Zhao, H. Hou, L. Guo, V. Murugadoss, H. Liu, Q. Shao, Q. Gao, T. Ding, R. Wei, Z. Guo, Iridium-based catalysts for solid polymer electrolyte electrocatalytic water splitting, ChemSusChem 12 (2019) 1576–1590, https://doi.org/10.1002/cssc.201802873.

[18] C. Spöri, J.T.H. Kwan, A. Bonakdarpour, D.P. Wilkinson, P. Strasser, The stability challenges of oxygen evolving catalysts: towards a common fundamental understanding and mitigation of catalyst degradation, Angew. Chem. - Int. Ed. 56 (2017) 5994–6021, https://doi.org/10.1002/anie.201608601.

[19] Q. Feng, X.Z. Yuan, G. Liu, B. Wei, Z. Zhang, H. Li, H. Wang, A review of proton exchange membrane water electrolysis on degradation mechanisms and mitigation strategies, J. Power Sources 366 (2017) 33–55, https://doi.org/10.1016/j.jpowsour.2017.09.006.

[20] E. Antolini, Iridium as catalyst and cocatalyst for oxygen evolution/reduction in acidic polymer electrolyte membrane electrolyzers and fuel cells, ACS Catal. 4 (2014) 1426–1440, https://doi.org/10.1021/cs4011875.

[21] M. Carmo, D.L. Fritz, J. Mergel, D. Stolten, A comprehensive review on PEM water electrolysis, Int. J. Hydrog. Energy 38 (2013) 4901–4934, https://doi.org/10.1016/j.ijhydene.2013.01.151.

[22] K. Ayers, N. Danilovic, R. Ouimet, M. Carmo, B. Pivovar, M. Bornstein, Perspectives on Low-Temperature Electrolysis and Potential for Renewable Hydrogen at Scale, (2019). https://doi.org/10.1146/annurev-chembioeng.

[23] L. Moriau, M. Smiljanić, A. Lončar, N. Hodnik, Supported iridium-based oxygen evolution reaction electrocatalysts - recent developments, ChemCatChem 14 (2022), https://doi.org/10.1002/cctc.202200586.

[24] B. Pivovar, M. Ruth, R. Ahluwalia, H2NEW: Hydrogen (H2) from Next-generation Electrolyzers of Water LTE Task 3c: System and Technoeconomic Analysis, 2022. https://www.hydrogen.energy.gov/pdfs/review22/p196d_ruth_2022_p.pdf.

[25] U. Babic, M. Suermann, F.N. Büchi, L. Gubler, T.J. Schmidt, Critical review—identifying critical gaps for polymer electrolyte water electrolysis development, J. Electrochem. Soc. 164 (2017) F387–F399, https://doi.org/10.1149/2.1441704jes.

[26] Z. Taie, X. Peng, D. Kulkarni, I.V. Zenyuk, A.Z. Weber, C. Hagen, N. Danilovic, Pathway to complete energy sector decarbonization with available iridium resources using ultralow loaded water electrolyzers, ACS Appl. Mater. Interfaces 12 (2020) 52701–52712, https://doi.org/10.1021/acsami.0c15687.

[27] M. Bernt, A. Siebel, H.A. Gasteiger, Analysis of voltage losses in PEM water electrolyzers with low platinum group metal loadings, J. Electrochem. Soc. 165 (2018) F305–F314, https://doi.org/10.1149/2.0641805jes.

[28] W. Sparber, W. Weiss, B. Sanner, L. Angelino, M. De Gregorio, N. Février, W. Haslinger, A. Kujbus, S. Landolina, G. Stryi-Hipp, W. Helden, Clean Hydrogen Joint Undertaking: Strategic Research and Innovation Agenda 2021–2027, 2021. ⟨www.clean-hydrogen.europa.eu/about-us/key-documents/strategic-research-and-innovation-agenda_en⟩.

[29] Fuel Cells and Hydrogen 2 Joint Undertaking: Addendum to the Multi - Annual Work Plan 2014 - 2020, 2018. ⟨www.fch.europa.eu/soa-and-targets⟩.

[30] Japanese Ministry of Economy Trade and Industry (METI), Strategy for Developing Hydrogen and Fuel-Cell Technologies, 2019. ⟨https://www.meti.go.jp/press/2019/09/20190918002/20190918002–2.pdf⟩.

[31] S. Geiger, O. Kasian, M. Ledendecker, E. Pizzutilo, A.M. Mingers, W.T. Fu, O. Diaz-Morales, Z. Li, T. Oellers, L. Fruchter, A. Ludwig, K.J.J. Mayrhofer, M.T. M. Koper, S. Cherevko, The stability number as a metric for electrocatalyst stability benchmarking, Nat. Catal. 1 (2018) 508–515, https://doi.org/10.1038/s41929-018-0085-6.

[32] S.M. Alia, S. Stariha, R.L. Borup, Electrolyzer durability at low catalyst loading and with dynamic operation, J. Electrochem. Soc. 166 (2019) F1164–F1172, https://doi.org/10.1149/2.0231915jes.

[33] H. Yu, L. Bonville, J. Jankovic, R. Maric, Microscopic insights on the degradation of a PEM water electrolyzer with ultra-low catalyst loading, Appl. Catal. B Environ. 260 (2020), 118194, https://doi.org/10.1016/j.apcatb.2019.118194.

[34] H. Ohno, S. Nohara, K. Kakinuma, M. Uchida, H. Uchida, Effect of electronic conductivities of iridium oxide/doped SnO2 oxygen-evolving catalysts on the polarization properties in proton exchange membrane water electrolysis, Catalysts 9 (2019) 5–7, https://doi.org/10.3390/catal9010074.

[35] C. Rozain, E. Mayousse, N. Guillet, P. Millet, Influence of iridium oxide loadings on the performance of PEM water electrolysis cells: part II – Advanced oxygen electrodes, Appl. Catal. B Environ. 182 (2016) 123–131, https://doi.org/10.1016/j.apcatb.2015.09.011.

[36] T.E. Graedel, J. Allwood, J.-P. Birat, B.K. Reck, S.F. Sibley, G. Sonnemann, M. Buchert, C. Hagelüken, Recycling Rates of Metals – A Status Report, 2011.

[37] C. Hagelüken, D. Goldmann, Recycling and circular economy—towards a closed loop for metals in emerging clean technologies, Miner. Econ. 35 (2022) 539–562, https://doi.org/10.1007/S13563-022-00319-1/FIGURES/11.

[38] Johnson Matthey PGMS Market Research, (2022).

[39] M. Carmo, G.P. Keeley, D. Holtz, T. Grube, M. Robinius, M. Müller, D. Stolten, PEM water electrolysis: innovative approaches towards catalyst separation, recovery and recycling, Int. J. Hydrog. Energy 44 (2019) 3450–3455, https://doi.org/10.1016/j.ijhydene.2018.12.030.

[40] Hydrogen Europe, Hydrogen Europe Position Paper: Delivering REPowerEU through a strong European hydrogen industry, 2022. ⟨https://hydrogeneurope.eu/wp-content/uploads/2022/05/2022.05.16_HE_PositionPaper_REPowerEU.pdf⟩.

[41] B. Pivovar, R. Boardman, H2NEW: Hydrogen (H2) from Next-generation Electrolyzers of Water Overview, 2021. ⟨https://www.hydrogen.energy.gov/pdfs/review21/p196_pivovar_boardman_2021_o.pdf⟩ (accessed March 10, 2023).

[42] M. Bernt, A. Hartig-Weiß, M.F. Tovini, H.A. El-Sayed, C. Schramm, J. Schröter, C. Gebauer, H.A. Gasteiger, Current challenges in catalyst development for PEM water electrolyzers, Chem. -Ing. -Tech. 92 (2020) 31–39, https://doi.org/10.1002/cite.201900101.

[43] M. Möckl, M.F. Ernst, M. Kornherr, F. Allebrod, M. Bernt, J. Byrknes, C. Eickes, C. Gebauer, A. Moskovtseva, H.A. Gasteiger, Durability testing of low-iridium PEM water electrolysis membrane electrode assemblies, J. Electrochem. Soc. 169 (2022), 064505, https://doi.org/10.1149/1945-7111/ac6d14.

[44] C.M. Zalitis, J. Sharman, E. Wright, A.R. Kucernak, Properties of the hydrogen oxidation reaction on Pt/C catalysts at optimised high mass transport conditions and its relevance to the anode reaction in PEFCs and cathode reactions in electrolysers, Electrochim. Acta 176 (2015) 763–776, https://doi.org/10.1016/j.electacta.2015.06.146.

[45] K.C. Neyerlin, W. Gu, J. Jorne, H.A. Gasteiger, Study of the exchange current density for the hydrogen oxidation and evolution reactions, J. Electrochem. Soc. 154 (2007) B631, https://doi.org/10.1149/1.2733987/XML.

[46] A.R. Kucernak, C.M. Zalitis, General models for the electrochemical hydrogen oxidation and hydrogen evolution reactions: theoretical derivation and experimental results under near mass-transport free conditions, J. Phys. Chem. C. 120 (2016) 10721–10745, https://doi.org/10.1021/acs.jpcc.6b00011.

[47] M. Bernt, H.A. Gasteiger, Influence of ionomer content in IrO 2 /TiO 2 electrodes on PEM water electrolyzer performance, J. Electrochem. Soc. 163 (2016) F3179–F3189, https://doi.org/10.1149/2.0231611jes.

[48] M. Mandal, M. Moore, M. Secanell, Measurement of the protonic and electronic conductivities of PEM water electrolyzer electrodes, ACS Appl. Mater. Interfaces 12 (2020) 49549–49562, https://doi.org/10.1021/acsami.0c12111.

[49] P. Lettenmeier, L. Wang, U. Golla-Schindler, P. Gazdzicki, N.A. Cañas, M. Handl, R. Hiesgen, S.S. Hosseiny, A.S. Gago, K.A. Friedrich, Nanosized IrOx-Ir catalyst with relevant activity for anodes of proton exchange membrane electrolysis produced by a cost-effective procedure, Angew. Chem. - Int. Ed. 55 (2016) 742–746, https://doi.org/10.1002/anie.201507626.

[50] M. Schalenbach, M. Carmo, D.L. Fritz, J. Mergel, D. Stolten, Pressurized PEM water electrolysis: efficiency and gas crossover, Int. J. Hydrog. Energy 38 (2013) 14921–14933, https://doi.org/10.1016/j.ijhydene.2013.09.013.

[51] M. Zatoń, J. Rozière, D.J. Jones, Current understanding of chemical degradation mechanisms of perfluorosulfonic acid membranes and their mitigation strategies: a review, Sustain. Energy Fuels. 1 (2017) 409–438, https://doi.org/10.1039/c7se00038c.

[52] R. Sood, S. Giancola, A. Donnadio, M. Zatoń, N. Donzel, J. Rozière, D.J. Jones, S. Cavaliere, Active electrospun nanofibers as an effective reinforcement for highly conducting and durable proton exchange membranes, J. Memb. Sci. 622 (2021), 119037, https://doi.org/10.1016/J.MEMSCI.2020.119037.

[53] F. Pantò, S. Siracusano, N. Briguglio, A.S. Aricò, Durability of a recombination catalyst-based membrane-electrode assembly for electrolysis operation at high current density, Appl. Energy 279 (2020), 115809, https://doi.org/10.1016/J.APENERGY.2020.115809.

[54] D.E. Barnwell, T.R. Ralph, P.A. Trew, Membrane Electrode Assembly, WO2009/040571, 2009.

[55] S. Schlick, M. Danilczuk, A.R. Drews, R.S. Kukreja, Scavenging of hydroxyl radicals by ceria nanoparticles: effect of particle size and concentration, J. Phys. Chem. C. 120 (2016) 6885–6890, https://doi.org/10.1021/acs.jpcc.6b00404.

[56] C. Klose, P. Trinke, T. Böhm, B. Bensmann, S. Vierrath, R. Hanke-Rauschenbach, S. Thiele, Membrane interlayer with Pt recombination particles for reduction of the anodic hydrogen content in PEM water electrolysis, J. Electrochem. Soc. 165 (2018) F1271–F1277, https://doi.org/10.1149/2.1241814jes.

[57] A. Stähler, M. Stähler, F. Scheepers, W. Lehnert, M. Carmo, Scalable implementation of recombination catalyst layers to mitigate gas crossover in PEM water electrolyzers, J. Electrochem. Soc. 169 (2022), 034522, https://doi.org/10.1149/1945-7111/ac5c9b.

[58] T. Schuler, R. De Bruycker, T.J. Schmidt, F.N. Büchi, Polymer electrolyte water electrolysis: correlating porous transport layer structural properties and performance: part I. Tomographic analysis of morphology and topology, J. Electrochem. Soc. 166 (2019) F270–F281, https://doi.org/10.1149/2.0561904JES/XML.

[59] Y. Wang, D.F. Ruiz Diaz, K.S. Chen, Z. Wang, X.C. Adroher, Materials, technological status, and fundamentals of PEM fuel cells – a review, Mater. Today 32 (2020) 178–203, https://doi.org/10.1016/j.mattod.2019.06.005.

[60] D.H. Swan, O.A. Velev, I.J. Kakwan, A.C. Ferreira, S. Srinivasan, A.J. Appleby, The proton exchange membrane fuel cell - a strong candidate as a power source for electric vehicles, 1991. ⟨https://www.google.com/url?sa=t&rct=j&q=&esrc=s&source=web&cd=&ved=2ahUKEwjVm97Z_r6AhXoTEEAHW3eBeY4FBAWegQIBhAB&url=https%3A%2F%2Fitspubs.ucdavis.edu%2Fdownload_pdf.php%3Fid%3D986&usg=AOvVaw2BIS6CGuK4AlZ8lc5v8O4d⟩ (accessed October 25, 2022).

[61] J. Spendelow, K. Epping Martin, D. Papageorgopoulos, DOE Hydrogen and Fuel Cells Program Record 9018 - Platinum Group Metal Loading, 2010. ⟨https://www.hydrogen.energy.gov/pdfs/9018_platinum_group.pdf⟩.

[62] S.S. Kocha, Principles of MEA preparation, in: W. Vielstich, A. Lamm, H. A. Gasteiger (Eds.), Handb. Fuel Cells – Fundam. Appl., Vol. 3, Wiley, Chichester, UK, 2003, pp. 538–565, https://www.wiley.com/en-gb/Handbook+of+Fuel+Cells%3A+Fundamentals%2C+Technology%2C+Applications%2C+4+Volume+Set-p-9780471499268 (accessed October 25, 2022).

[63] B. James, 2021 DOE Hydrogen and Fuel Cells Program Review Presentation, 2021. https://www.hydrogen.energy.gov/pdfs/review21/fc163_james_2021_o.pdf.

[64] A. Kongkanand, M.F. Mathias, The priority and challenge of high-power performance of low-platinum proton-exchange membrane fuel cells, J. Phys. Chem. Lett. 7 (2016) 1127–1137, https://doi.org/10.1021/acs.jpclett.6b00216.

[65] M.S. Thomassen, A.O. Barnet, A method for Producing Hydrogen in a PEM water electrolyser system, pem water electrolyser, Cell Stack Syst. (2021) EP3649276, https://doi.org/10.1016/j.pnucene.2007.11.029.

[66] H. Xu, B. Rasimick, A. Stocks, B. Pivovar, S. Alia, K.C. Neyerlin, K. Lewinski, S. Luopa, High-Performance, Long-Lifetime Catalysts for Proton Exchange Membrane Electrolysis, 2015. ⟨www.hydrogen.energy.gov⟩.

[67] F. Hegge, F. Lombeck, E. Cruz Ortiz, L. Bohn, M. Von Holst, M. Kroschel, J. Hübner, M. Breitwieser, P. Strasser, S. Vierrath, Efficient and stable low iridium loaded anodes for PEM water electrolysis made possible by nanofiber interlayers, ACS Appl. Energy Mater. 3 (2020) 8276–8284, https://doi.org/10.1021/acsaem.0c00735.

[68] S. Siracusano, V. Baglio, S.A. Grigoriev, L. Merlo, V.N. Fateev, A.S. Aricò, The influence of iridium chemical oxidation state on the performance and durability of oxygen evolution catalysts in PEM electrolysis, J. Power Sources 366 (2017) 105–114, https://doi.org/10.1016/j.jpowsour.2017.09.020.

[69] S. Siracusano, N. Hodnik, P. Jovanovic, F. Ruiz-Zepeda, M. Šala, V. Baglio, A. S. Aricò, New insights into the stability of a high performance nanostructured catalyst for sustainable water electrolysis, Nano Energy 40 (2017) 618–632, https://doi.org/10.1016/j.nanoen.2017.09.014.

[70] X. Min, Y. Shi, Z. Lu, L. Shen, T.O. Ogundipe, P. Gupta, C. Wang, C. Guo, Z. Wang, H. Tan, S. Mukerjee, C. Yan, High performance and cost-effective supported IrOx catalyst for proton exchange membrane water electrolysis, Electrochim. Acta 385 (2021), 138391, https://doi.org/10.1016/j.electacta.2021.138391.

[71] L. Bertuccioli, A. Chan, D. Hart, F. Lehner, B. Madden, E. Standen, Fuel Cells and Hydrogen Joint Undertaking: Study on Development of Water Electrolysis in the EU, 2014. https://www.fch.europa.eu/sites/default/files/FCHJUElectrolysisStudy_FullReport (ID 199214).pdf.

[72] G. Li, S. Li, M. Xiao, J. Ge, C. Liu, W. Xing, Nanoporous IrO2 catalyst with enhanced activity and durability for water oxidation owing to its micro/mesoporous structure, Nanoscale 9 (2017) 9291–9298, https://doi.org/10.1039/c7nr02899g.

[73] S. Siracusano, N. Van Dijk, E. Payne-Johnson, V. Baglio, A.S. Aricò, Nanosized IrOx and IrRuOx electrocatalysts for the O2 evolution reaction in PEM water electrolysers, Appl. Catal. B Environ. 164 (2015) 488–495, https://doi.org/10.1016/j.apcatb.2014.09.005.

[74] F. Bizzotto, J. Quinson, A. Zana, J.J.K. Kirkensgaard, A. Dworzak, M. Oezaslan, M. Arenz, Ir nanoparticles with ultrahigh dispersion as oxygen evolution reaction (OER) catalysts: synthesis and activity benchmarking, Catal. Sci. Technol. 9 (2019) 6345–6356, https://doi.org/10.1039/c9cy01728c.

[75] J. Ruiz Esquius, D.J. Morgan, I. Spanos, D.G. Hewes, S.J. Freakley, G. J. Hutchings, Effect of base on the facile hydrothermal preparation of highly active IrOx oxygen evolution catalysts, ACS Appl. Energy Mater. 3 (2020) 800–809, https://doi.org/10.1021/acsaem.9b01642.

[76] C. Rozain, E. Mayousse, N. Guillet, P. Millet, Influence of iridium oxide loadings on the performance of PEM water electrolysis cells: part I-Pure IrO2-based anodes, Appl. Catal. B Environ. 182 (2016) 153–160, https://doi.org/10.1016/j.apcatb.2015.09.013.

[77] Y. Sugita, T. Tamaki, H. Kuroki, T. Yamaguchi, Connected iridium nanoparticle catalysts coated onto silica with high density for oxygen evolution in polymer electrolyte water electrolysis, Nanoscale Adv. 2 (2020) 171–175, https://doi.org/10.1039/c9na00568d.

[78] H.S. Oh, H.N. Nong, T. Reier, M. Gliech, P. Strasser, Oxide-supported Ir nanodendrites with high activity and durability for the oxygen evolution reaction in acid PEM water electrolyzers, Chem. Sci. 6 (2015) 3321–3328, https://doi.org/10.1039/c5sc00518c.

[79] G. Liu, J. Xu, Y. Wang, X. Wang, An oxygen evolution catalyst on an antimony doped tin oxide nanowire structured support for proton exchange membrane liquid water electrolysis, J. Mater. Chem. A 3 (2015) 20791–20800, https://doi.org/10.1039/c5ta02942b.

[80] A. Hartig-Weiss, M. Miller, H. Beyer, A. Schmitt, A. Siebel, A.T.S. Freiberg, H. A. Gasteiger, H.A. El-Sayed, Iridium oxide catalyst supported on antimony-doped tin oxide for high oxygen evolution reaction activity in acidic media, ACS Appl. Nano Mater. 3 (2020) 2185–2196, https://doi.org/10.1021/acsanm.9b02230.

[81] H. Lv, G. Zhang, C. Hao, C. Mi, W. Zhou, D. Yang, B. Li, C. Zhang, Activity of IrO2 supported on tantalum-doped TiO2 electrocatalyst for solid polymer electrolyte water electrolyzer, RSC Adv. 7 (2017) 40427–40436, https://doi.org/10.1039/c7ra06534e.

[82] G. Jiang, H. Yu, Y. Li, D. Yao, J. Chi, S. Sun, Z. Shao, Low-loading and highly stable membrane electrode based on an Ir@WOxNR ordered array for PEM water electrolysis, ACS Appl. Mater. Interfaces 13 (2021) 15073–15082, https://doi.org/10.1021/acsami.0c20791.
[83] M. Ledendecker, S. Geiger, K. Hengge, J. Lim, S. Cherevko, A.M. Mingers, D. Göhl, G.V. Fortunato, D. Jalalpoor, F. Schüth, C. Scheu, K.J.J. Mayrhofer, Towards maximized utilization of iridium for the acidic oxygen evolution reaction, Nano Res 12 (2019) 2275–2280, https://doi.org/10.1007/s12274-019-2383-y.
[84] C. Van Pham, M. Bühler, J. Knöppel, M. Bierling, D. Seeberger, D. Escalera-López, K.J.J. Mayrhofer, S. Cherevko, S. Thiele, IrO2 coated TiO2 core-shell microparticles advance performance of low loading proton exchange membrane water electrolyzers, Appl. Catal. B Environ. 269 (2020), 118762, https://doi.org/10.1016/j.apcatb.2020.118762.
[85] H.N. Nong, L. Gan, E. Willinger, D. Teschner, P. Strasser, IrOx core-shell nanocatalysts for cost- and energy-efficient electrochemical water splitting, Chem. Sci. 5 (2014) 2955–2963, https://doi.org/10.1039/c4sc01065e.
[86] H.N. Nong, T. Reier, H.S. Oh, M. Gliech, P. Paciok, T.H.T. Vu, D. Teschner, M. Heggen, V. Petkov, R. Schlögl, T. Jones, P. Strasser, A unique oxygen ligand environment facilitates water oxidation in hole-doped IrNiOx core–shell electrocatalysts, Nat. Catal. 1 (2018) 841–851, https://doi.org/10.1038/s41929-018-0153-y.
[87] J. Zhang, Z. Chen, C. Liu, J. Zhao, S. Liu, D. Rao, A. Nie, Y. Chen, Y. Deng, W. Hu, Hierarchical iridium-based multimetallic alloy with double-core-shell architecture for efficient overall water splitting, Sci. China Mater. 63 (2020) 249–257, https://doi.org/10.1007/s40843-019-1176-6.
[88] K.A. Lewinski, D. van der Vliet, S.M. Luopa, NSTF advances for PEM electrolysis - the effect of alloying on activity of NSTF electrolyzer catalysts and performance of NSTF based PEM electrolyzers, ECS Trans. 69 (2015) 893–917, https://doi.org/10.1149/06917.0893ecst.
[89] M.K. Debe, Tutorial on the fundamental characteristics and practical properties of nanostructured thin film (NSTF) catalysts, J. Electrochem. Soc. 160 (2013) F522–F534, https://doi.org/10.1149/2.049306JES/XML.
[90] S. Chatterjee, X. Peng, S. Intikhab, G. Zeng, N.N. Kariuki, D.J. Myers, N. Danilovic, J. Snyder, Nanoporous iridium nanosheets for polymer electrolyte membrane electrolysis, Adv. Energy Mater. 11 (2021) 2101438, https://doi.org/10.1002/aenm.202101438.
[91] S.M. Alia, S. Shulda, C. Ngo, S. Pylypenko, B.S. Pivovar, Iridium-based nanowires as highly active, oxygen evolution reaction electrocatalysts, ACS Catal. 8 (2018) 2111–2120, https://doi.org/10.1021/acscatal.7b03787.
[92] A.W. Jensen, G.W. Sievers, K.D. Jensen, J. Quinson, J.A. Arminio-Ravelo, V. Brüser, M. Arenz, M. Escudero-Escribano, Self-supported nanostructured iridium-based networks as highly active electrocatalysts for oxygen evolution in acidic media, J. Mater. Chem. A 8 (2020) 1066–1071, https://doi.org/10.1039/c9ta12796h.
[93] Y.T. Kim, P.P. Lopes, S.A. Park, A.Y. Lee, J. Lim, H. Lee, S. Back, Y. Jung, N. Danilovic, V. Stamenkovic, J. Erlebacher, J. Snyder, N.M. Markovic, Balancing activity, stability and conductivity of nanoporous core-shell iridium/iridium oxide oxygen evolution catalysts, Nat. Commun. 8 (2017) 1–8, https://doi.org/10.1038/s41467-017-01734-7.
[94] W. Hu, Y. Wang, X. Hu, Y. Zhou, S. Chen, Three-dimensional ordered macroporous IrO2 as electrocatalyst for oxygen evolution reaction in acidic medium, J. Mater. Chem. 22 (2012) 6010–6016, https://doi.org/10.1039/c2jm16506f.
[95] L. Yang, G. Yu, X. Ai, W. Yan, H. Duan, W. Chen, X. Li, T. Wang, C. Zhang, X. Huang, J.S. Chen, X. Zou, Efficient oxygen evolution electrocatalysis in acid by a perovskite with face-sharing IrO6 octahedral dimers, Nat. Commun. 9 (2018) 5236, https://doi.org/10.1038/s41467-018-07678-w.
[96] T. Reier, Z. Pawolek, S. Cherevko, M. Bruns, T. Jones, D. Teschner, S. Selve, A. Bergmann, H.N. Nong, R. Schlögl, K.J.J. Mayrhofer, P. Strasser, Molecular insight in structure and activity of highly efficient, low-Ir Ir-Ni oxide catalysts for electrochemical water splitting (OER), J. Am. Chem. Soc. 137 (2015) 13031–13040, https://doi.org/10.1021/jacs.5b07788.
[97] G. Jiang, H. Yu, J. Hao, J. Chi, Z. Fan, D. Yao, B. Qin, Z. Shao, An effective oxygen electrode based on Ir 0.6 Sn 0.4 O 2 for PEM water electrolyzers, J. Energy Chem. 39 (2019) 23–28, https://doi.org/10.1016/j.jechem.2019.01.011.
[98] T. Audichon, E. Mayousse, S. Morisset, C. Morais, C. Comminges, T.W. Napporn, K.B. Kokoh, Electroactivity of RuO2–IrO2 mixed nanocatalysts toward the oxygen evolution reaction in a water electrolyzer supplied by a solar profile, Int. J. Hydrog. Energy 39 (2014) 16785–16796, https://doi.org/10.1016/J.IJHYDENE.2014.07.170.
[99] S. Siracusano, V. Baglio, A. Stassi, R. Ornelas, V. Antonucci, A.S. Aric, Investigation of IrO2 electrocatalysts prepared by a sulfite-couplex route for the O2 evolution reaction in solid polymer electrolyte water electrolyzers, Int. J. Hydrog. Energy 36 (2011) 7822–7831, https://doi.org/10.1016/j.ijhydene.2010.12.080.
[100] H. Su, V. Linkov, B.J. Bladergroen, Membrane electrode assemblies with low noble metal loadings for hydrogen production from solid polymer electrolyte water electrolysis, Int. J. Hydrog. Energy 38 (2013) 9601–9608, https://doi.org/10.1016/j.ijhydene.2013.05.099.
[101] X. Wang, Z.G. Shao, G. Li, L. Zhang, Y. Zhao, W. Lu, B. Yi, Preparation and characterization of partial-cocrystallized catalyst-coated membrane for solid polymer electrolyte water electrolysis, Int. J. Hydrog. Energy 38 (2013) 9057–9064, https://doi.org/10.1016/j.ijhydene.2013.05.095.
[102] H.S. Oh, H.N. Nong, T. Reier, A. Bergmann, M. Gliech, J. Ferreira De Araújo, E. Willinger, R. Schlögl, D. Teschner, P. Strasser, Electrochemical catalyst-support effects and their stabilizing role for irox nanoparticle catalysts during the oxygen evolution reaction, J. Am. Chem. Soc. 138 (2016) 12552–12563, https://doi.org/10.1021/jacs.6b07199.
[103] H.N. Nong, H.S. Oh, T. Reier, E. Willinger, M.G. Willinger, V. Petkov, D. Teschner, P. Strasser, Oxide-supported IrNiOx core-shell particles as efficient, cost-effective, and stable catalysts for electrochemical water splitting, Angew. Chem. Int. Ed. 54 (2015) 2975–2979, https://doi.org/10.1002/anie.201411072.
[104] E. Oakton, D. Lebedev, A. Fedorov, F. Krumeich, J. Tillier, O. Sereda, T. J. Schmidt, C. Copéret, A simple one-pot Adams method route to conductive high surface area IrO2-TiO2 materials, New J. Chem. 40 (2016) 1834–1838, https://doi.org/10.1039/c5nj02400e.
[105] J. Zhang, F. Coms, S. Kumaraguru, Necessity to avoid titanium oxide as electrocatalyst support in PEM fuel cells: a membrane durability study, J. Electrochem. Soc. 168 (2021), 024520, https://doi.org/10.1149/1945-7111/abe5e9.
[106] S. Geiger, O. Kasian, A.M. Mingers, K.J.J. Mayrhofer, S. Cherevko, Stability limits of tin-based electrocatalyst supports, Sci. Rep. 7 (2017) 4595, https://doi.org/10.1038/s41598-017-04079-9.
[107] S. Cherevko, T. Reier, A.R. Zeradjanin, Z. Pawolek, P. Strasser, K.J.J. Mayrhofer, Stability of nanostructured iridium oxide electrocatalysts during oxygen evolution reaction in acidic environment, Electrochem. Commun. 48 (2014) 81–85, https://doi.org/10.1016/j.elecom.2014.08.027.
[108] P. Jovanovič, N. Hodnik, F. Ruiz-Zepeda, I. Arčon, B. Jozinović, M. Zorko, M. Bele, M. Šala, V.S. Šelih, S. Hočevar, M. Gaberščček, Electrochemical dissolution of iridium and iridium oxide particles in acidic media: transmission electron microscopy, electrochemical flow cell coupled to inductively coupled plasma mass spectrometry, and X-ray absorption spectroscopy study, J. Am. Chem. Soc. 139 (2017) 12837–12846, https://doi.org/10.1021/JACS.7B08071.
[109] O. Kasian, S. Geiger, T. Li, J.P. Grote, K. Schweinar, S. Zhang, C. Scheu, D. Raabe, S. Cherevko, B. Gault, K.J.J. Mayrhofer, Degradation of iridium oxides via oxygen evolution from the lattice: correlating atomic scale structure with reaction mechanisms, Energy Environ. Sci. 12 (2019) 3548–3555, https://doi.org/10.1039/c9ee01872g.
[110] F. Claudel, L. Dubau, G. Berthomé, L. Sola-Hernandez, C. Beauger, L. Piccolo, F. Maillard, Degradation mechanisms of oxygen evolution reaction electrocatalysts: a combined identical-location transmission electron microscopy and X-ray photoelectron spectroscopy study, ACS Catal. 9 (2019) 4688–4698, https://doi.org/10.1021/acscatal.9b00280.
[111] N. Danilovic, R. Subbaraman, K.C. Chang, S.H. Chang, Y. Kang, J. Snyder, A. P. Paulikas, D. Strmcnik, Y.T. Kim, D. Myers, V.R. Stamenkovic, N.M. Markovic, Using surface segregation to design stable Ru-Ir oxides for the oxygen evolution reaction in acidic environments, Angew. Chem. 126 (2014) 14240–14245, https://doi.org/10.1002/ANGE.201406455.
[112] Z. Ma, Y. Zhang, S. Liu, W. Xu, L. Wu, Y.C. Hsieh, P. Liu, Y. Zhu, K. Sasaki, J. N. Renner, K.E. Ayers, R.R. Adzic, J.X. Wang, Reaction mechanism for oxygen evolution on RuO2, IrO2, and RuO2@IrO2 core-shell nanocatalysts, J. Electroanal. Chem. 819 (2018) 296–305, https://doi.org/10.1016/J.JELECHEM.2017.10.062.
[113] O. Kasian, S. Geiger, P. Stock, G. Polymeros, B. Breitbach, A. Savan, A. Ludwig, S. Cherevko, K.J.J. Mayrhofer, On the origin of the improved ruthenium stability in RuO 2 –IrO 2 mixed oxides, J. Electrochem. Soc. 163 (2016) F3099–F3104, https://doi.org/10.1149/2.0131611jes.
[114] A. Grimaud, A. Demortiere, M. Saubanere, W. Dachraoui, M. Duchamp, M. L. Doublet, J.M. Tarascon, Activation of surface oxygen sites on an iridium-based model catalyst for the oxygen evolution reaction, 2016 21, Nat. Energy 2 (2016) 1–10, https://doi.org/10.1038/nenergy.2016.189.
[115] W. Sun, Z. Wang, Z. Zhou, Y. Wu, W.Q. Zaman, M. Tariq, L.M. Cao, X.Q. Gong, J. Yang, A promising engineering strategy for water electro-oxidation iridate catalysts: via coordination distortion, Chem. Commun. 55 (2019) 5801–5804, https://doi.org/10.1039/c9cc02447f.
[116] W. Sun, Y. Song, X.Q. Gong, L.M. Cao, J. Yang, Hollandite structure Kx≈0.25IrO2 catalyst with highly efficient oxygen evolution reaction, ACS Appl. Mater. Interfaces 8 (2016) 820–826, https://doi.org/10.1021/acsami.5b10159.
[117] E. Willinger, C. Massué, R. Schlögl, M.G. Willinger, Identifying key structural features of IrOx water splitting catalysts, J. Am. Chem. Soc. 139 (2017) 12093–12101, https://doi.org/10.1021/jacs.7b07079.
[118] O. Diaz-Morales, S. Raaijman, R. Kortlever, P.J. Kooyman, T. Wezendonk, J. Gascon, W.T. Fu, M.T.M. Koper, Iridium-based double perovskites for efficient water oxidation in acid media, Nat. Commun. 7 (2016) 1–6, https://doi.org/10.1038/ncomms12363.
[119] K. Sardar, E. Petrucco, C.I. Hiley, J.D.B. Sharman, P.P. Wells, A.E. Russell, R. J. Kashtiban, J. Sloan, R.I. Walton, Water-splitting electrocatalysis in acid conditions using ruthenate-iridate pyrochlores, Angew. Chem. 126 (2014) 11140–11144, https://doi.org/10.1002/ange.201406668.
[120] H. Yu, N. Danilovic, Y. Wang, W. Willis, A. Poozhikunnath, L. Bonville, C. Capuano, K. Ayers, R. Maric, Nano-size IrOx catalyst of high activity and stability in PEM water electrolyzer with ultra-low iridium loading, Appl. Catal. B Environ. 239 (2018) 133–146, https://doi.org/10.1016/j.apcatb.2018.07.064.
[121] P. Aßmann, A.S. Gago, P. Gazdzicki, K.A. Friedrich, M. Wark, Toward developing accelerated stress tests for proton exchange membrane electrolyzers, Curr. Opin. Electrochem. 21 (2020) 225–233, https://doi.org/10.1016/J.COELEC.2020.02.024.
[122] C. Spöri, C. Brand, M. Kroschel, P. Strasser, Accelerated degradation protocols for iridium-based oxygen evolving catalysts in water splitting devices, J. Electrochem. Soc. 168 (2021), 034508, https://doi.org/10.1149/1945-7111/ABEB61.

[123] A. Weiß, M. Bernt, A. Siebel, P.J. Rheinländer, H.A. Gasteiger, Accelerated degradation Test in PEM water electrolysis, MA2017-02, ECS Meet. Abstr. (2017) 1648, https://doi.org/10.1149/ma2017-02/37/1648.
[124] A. Weiß, A. Siebel, M. Bernt, T.-H. Shen, V. Tileli, H.A. Gasteiger, Impact of intermittent operation on lifetime and performance of a PEM water electrolyzer, J. Electrochem. Soc. 166 (2019) F487–F497, https://doi.org/10.1149/2.0421908JES/XML.
[125] S.M. Alia, K.S. Reeves, H. Yu, J. Park, N. Kariuki, A.J. Kropf, D.J. Myers, D. A. Cullen, Electrolyzer performance loss from accelerated stress tests and corresponding changes to catalyst layers and interfaces, J. Electrochem. Soc. 169 (2022), 054517, https://doi.org/10.1149/1945-7111/AC697E.
[126] M.J. Burch, K.A. Lewinski, M.I. Buckett, S. Luopa, F. Sun, E.J. Olson, A. J. Steinbach, A novel work-flow to study Ir electrode thinning and dissolution in proton exchange membrane water electrolyzers, J. Power Sources 500 (2021), 229978, https://doi.org/10.1016/j.jpowsour.2021.229978.
[127] P. Lettenmeier, R. Wang, R. Abouatallah, S. Helmly, T. Morawietz, R. Hiesgen, S. Kolb, F. Burggraf, J. Kallo, A.S. Gago, K.A. Friedrich, Durable membrane electrode assemblies for proton exchange membrane electrolyzer systems operating at high current densities, Electrochim. Acta 210 (2016) 502–511, https://doi.org/10.1016/j.electacta.2016.04.164.
[128] S.A. Grigoriev, K.A. Dzhus, D.G. Bessarabov, P. Millet, Failure of PEM water electrolysis cells: case study involving anode dissolution and membrane thinning, Int. J. Hydrog. Energy 39 (2014) 20440–20446, https://doi.org/10.1016/J.IJHYDENE.2014.05.043.
[129] S.F. Zaccarine, M. Shviro, J.N. Weker, M.J. Dzara, J. Foster, M. Carmo, S. Pylypenko, Multi-scale multi-technique characterization approach for analysis of PEM electrolyzer catalyst layer degradation, J. Electrochem. Soc. 169 (2022), 064502, https://doi.org/10.1149/1945-7111/AC7258.
[130] O. Kasian, S. Geiger, K.J.J. Mayrhofer, S. Cherevko, Electrochemical on-line ICP-MS in electrocatalysis research, Chem. Rec. 19 (2019) 2130–2142, https://doi.org/10.1002/tcr.201800162.
[131] M. Escudero-Escribano, A.F. Pedersen, E.A. Paoli, R. Frydendal, D. Friebel, P. Malacrida, J. Rossmeisl, I.E.L. Stephens, I. Chorkendorff, Importance of surface IrOx in stabilizing RuO2 for oxygen evolution, J. Phys. Chem. B. 122 (2018) 947–955, https://doi.org/10.1021/acs.jpcb.7b07047.
[132] H.A. El-Sayed, A. Weiß, L.F. Olbrich, G.P. Putro, H.A. Gasteiger, OER catalyst stability investigation using RDE technique: a stability measure or an artifact? J. Electrochem. Soc. 166 (2019) F458–F464, https://doi.org/10.1149/2.0301908jes.
[133] M. Fathi Tovini, A. Hartig-Weiß, H.A. Gasteiger, H.A. El-Sayed, The discrepancy in oxygen evolution reaction catalyst lifetime explained: RDE vs MEA - dynamicity within the catalyst layer matters, J. Electrochem. Soc. 168 (2021), 014512, https://doi.org/10.1149/1945-7111/abdcc9.
[134] J. Knöppel, M. Möckl, D. Escalera-López, K. Stojanovski, M. Bierling, T. Böhm, S. Thiele, M. Rzepka, S. Cherevko, On the limitations in assessing stability of oxygen evolution catalysts using aqueous model electrochemical cells, Nat. Commun. 12 (2021) 1–9, https://doi.org/10.1038/s41467-021-22296-9.
[135] K. Ehelebe, D. Escalera-López, S. Cherevko, Limitations of aqueous model systems in the stability assessment of electrocatalysts for oxygen reactions in fuel cell and electrolyzers, Curr. Opin. Electrochem. 29 (2021), 100832, https://doi.org/10.1016/J.COELEC.2021.100832.
[136] US DoE, Appendix A: FCTT AST and Polarization Curve Protocols for PEMFCs, 2013. ⟨https://www.energy.gov/sites/default/files/2015/08/f25/fcto_dwg_usdrive_fctt_accelerated_stress_tests_jan2013.pdf⟩ (accessed November 2, 2022).
[137] US DoE, Rotating Disk-Electrode Aqueous Electrolyte Accelerated Stress Tests for PGM Electrocatalyst/Support Durability Evaluation, 2011. ⟨https://www.energy.gov/sites/prod/files/2015/08/f25/fcto_dwg_pgm_electrocatalyst_support_aqueous_ast.pdf⟩ (accessed November 2, 2022).
[138] A. Lončar, D. Escalera-López, S. Cherevko, N. Hodnik, Inter-relationships between oxygen evolution and iridium dissolution mechanisms, Angew. Chem. Int. Ed. 61 (2022), https://doi.org/10.1002/anie.202114437.
[139] X. Tan, J. Shen, N. Semagina, M. Secanell, Decoupling structure-sensitive deactivation mechanisms of Ir/IrOx electrocatalysts toward oxygen evolution reaction, J. Catal. 371 (2019) 57–70, https://doi.org/10.1016/j.jcat.2019.01.018.
[140] O. Kasian, J.-P. Grote, S. Geiger, S. erhiy Cherevko, nd J. Karl J. Mayrhofer, S. Cherevko, K.J.J. Mayrhofer, D. Cherevko, The Common Intermediates of Oxygen Evolution and Dissolution Reactions during Water Electrolysis on Iridium, (n.d.). https://doi.org/10.1002/ange.201709652.
[141] A.P. Dam, G. Papakonstantinou, K. Sundmacher, On the role of microkinetic network structure in the interplay between oxygen evolution reaction and catalyst dissolution, Sci. Rep. 101 (10) (2020) 1–13, https://doi.org/10.1038/s41598-020-69723-3.
[142] C. Klose, T. Saatkamp, A. Münchinger, L. Bohn, G. Titvinidze, M. Breitwieser, K. D. Kreuer, S. Vierrath, All-Hydrocarbon MEA for PEM Water Electrolysis Combining Low Hydrogen Crossover and High Efficiency, Adv. Energy Mater. 10 (2020) 1903995. https://doi.org/10.1002/AENM.201903995.